miR-23b neutralization in brain endothelium promotes blood-brain barrier repair through Wnt/β-catenin dependent and independent mechanisms

Victor Anthony Martinez[1], Sara Nakanishi[1], Johannes Daugaard Krog[1], Iben Daugaard Krog[1], Douglas Jury[1], Brian Lawson[1], Jacob Körbelin[2], Dritan Agalliu[3,4] and Irene Munk Pedersen[1*]

[1]Scintillon Aging Research Center, Scintillon Research Institute, San Diego, CA 92121, USA
[2]ENDomics Lab, Department of Oncology, Hematology and Bone Marrow Transplantation, University Medical Center Hamburg-Eppendorf, Hamburg, Germany
[3]Departments of Neurology and [4]Pathology and Cell Biology, Columbia University Irving Medical Center, New York, NY, USA

Running Title: anti-miR-23b enhances BBB function and repair.

***Corresponding author:**
Irene Munk Pedersen, Ph.D. Email: imp@scintillon.org
The Scintillon Research Institute
Scintillon Aging Research Center
6868 Nancy Drive
San Diego, California, 92121, USA

Lead contact:
Irene Munk Pedersen, Ph.D. Email: imp@scintillon.org

Total word count: 12,054

ABSTRACT

Disruption of the blood-brain barrier (BBB) is an early and critical event in the pathogenesis of stroke and other central nervous system (CNS) disorders. Yet, therapeutic strategies to restore BBB integrity remain limited. Using an unbiased anti-miR library screen, we identify miR-23b as a negative regulator of BBB integrity in brain endothelial cells (BECs). Targeted inhibition of miR-23b with anti-miR -23b in BECs enhances junction protein expression, suppresses transcellular transport, and improves barrier function via Wnt/β-catenin-dependent and -independent mechanisms. In a 3D microfluidic model, anti-miR-23b accelerates vessel maturation, enhances resilience to ischemic injury, and facilitates BBB repair. AAVBR1-mediated delivery of anti-miR-23b to brain endothelium reduces BBB leakage, infarct volume, neurological deficits, and mortality in the rodent transient middle cerebral artery occlusion (tMCAo). Thus, miR-23b is a critical regulator of cerebrovascular integrity, and anti-miR-23b may be a promising novel RNA-based therapeutic to enhance BBB repair in stroke and other CNS disorders.

KEYWORDS:

blood-brain barrier (BBB), miR-23b/anti-miR-23b, Wnt/β-catenin signaling, ischemic stroke, 3D modeling, RNA therapeutics

LIST OF NONSTANDARD ABBREVIATIONS AND NONSTANDARD ACRONYMS

AAV: adeno-associated virus, AJ: adherens junction, BBB: blood-brain barrier, **BEC**: brain endothelial cells, **BI**: barrier integrity, **CNS**: central nervous system, **miRs**: microRNA, **NVU**: neurovascular unit, **OGD**: oxygen-glucose deprivation, **PLVAP**: plasmalemma vesicle-associated protein, **TEER**: trans-endothelial electrical resistance, **TJP**: tight junction protein, **tMCAo**: transient middle cerebral artery occlusion

INTRODUCTION

Neurological disorders with a prominent vascular component, such as stroke and Alzheimer's disease (AD), represent a major healthcare burden. These diseases have heterogeneous pathobiology derived from multiple risk factors, many directly or indirectly related to blood-brain barrier (BBB) impairment[1,2]. Stroke affects over 15 million people worldwide each year, with most cases being ischemic and often leading to death or long-term disability[3,4]. Disruption of the BBB, one of the earliest events in stroke, strongly correlates with poor outcomes[5-7]. Aging, associated with BBB dysfunction, is a major risk factor for these diseases[8-17]. Changes in blood plasma protein composition resulting from transcriptional changes in brain endothelial cells (BECs), and systemic chronic inflammation, are thought to be contributing factors for age-related BBB dysfunction[18-23]. Additionally, increased BBB permeability has been found to predict cognitive deficits in older adults, and is considered an early indicator of impairments, dementia, and AD[12-15].

The BBB is a highly selective semipermeable barrier that regulates the passage of substances between the blood and the brain. Its complex and dynamic structure is formed by tight junctions (TJs) composed of proteins such as Claudin-5, Occludin, and ZO-1 in BECs and a low rate of caveolar transport. Supporting cells, including pericytes (PCs), astrocytes (ACs), and the capillary vascular basement membrane (vBM), contribute to the structural and functional architecture of the BBB (reviewed in[24]). Despite the growing understanding of the BBB's role in CNS diseases, many unanswered questions remain about the timing and mechanisms of BBB dysfunction in ischemic stroke and the optimal therapeutic strategies to target it.

The Wnt/β-catenin pathway and associated downstream transcription factors are critical for CNS angiogenesis, proliferation, survival, and BBB formation through stabilization and nuclear translocation of β-catenin (reviewed in[24]). Dysregulation of this pathway has also been implicated in stroke, AD, and MS[25-29]. More recently, small non-coding RNAs modulating post-transcriptional gene expression, microRNAs (miRs), have emerged as important regulators of BEC function and BBB integrity[30-32]. miRs exemplify the growing recognition that non-coding RNAs can rival proteins in regulatory significance. miRs are loaded onto Argonaute proteins and function as 21–24 nucleotide guide RNAs that recognize target mRNAs via partial base pairing, leading to mRNA destabilization or translational repression[33,34]. Target recognition is largely governed by a short six-nucleotide "seed" sequence (positions 2–7), which binds complementary sites in target mRNAs[33,35]. Nearly the entire human transcriptome is subject to miR regulation, placing these molecules as central participants in gene control networks[36]. We and

others have shown that miRs can be induced by cytokines such as interferon-β (IFN-β) and tumor necrosis factor-α (TNF-α), playing critical roles in modulating inflammation[37-40]. Approximately 70% of all miRs are expressed in the mammalian brain, underscoring their vital importance in maintaining brain homeostasis and potentially contributing to CNS disease. Not surprisingly, miRs are increasingly recognized as promising next-generation drug targets across various diseases, including neurological disorders.

Here, we employ a non-biased anti-miR lentiviral screen strategy and identify miR-23b/anti-miR-23b as a key regulator of BBB (dys)function in BECs. Using gain- and loss-of-function approaches, we explore the timing and mechanisms underlying the regulation of BBB function in healthy BECs and then under ischemic stroke conditions using an *in vitro* human 3D BBB microfluidic model and an *in vivo* rodent model. Our data demonstrate that anti-miR-23b enhances BBB properties by regulating junctional proteins, transcytosis, and Wnt/β-catenin signaling, thus improving outcomes in both ischemic stroke models. The findings have physiological and clinical relevance as miRs and their inhibitors become potential therapeutics.

METHODS

Cell Culture

Mouse lung endothelial cells (mLEC; C57-6011, Cell Biologics, Chicago, IL, USA) were maintained in complete mouse EC media (M1168, Cell Biologics, Chicago, IL, USA) and 10% FBS (FB-02, Omega Scientific, Tarzana, CA, USA). Human lung EC (human LEC; #3000, ScienCell, Carlsbad, CA, USA) were maintained on plates coated with 10 µg/ml fibronectin (F2006, Sigma-Aldrich, St. Louis, MO, USA) in EC media (1001, ScienCell). Primary human Brain Microvascular Endothelial Cells (HBMEC, ACBRI76, Cell Systems, Kirkland, WA, USA) were cultured on 15 µg/ml fibronectin coated T75 flasks (353112, Corning, Corning, NY, USA) in EndoGro-MV Complete Medium (SCME004, Sigma-Aldrich, St. Louis, MO, USA) supplemented with 5ng/mL bFGF (3718-FB-025, R&D systems, Minneapolis, MN, USA). Human Cerebral Microvascular Endothelial Cell line (hCMEC/D3; SCC066, Sigma-Aldrich, St. Louis, MO, USA) cells were grown on Rat Collagen Type I (C3867-1VL, Sigma-Aldrich, St. Louis, MO, USA) coated T75 flasks in EndoGro-MV complete Medium supplemented with bFGF. Primary Human Umbilical Cord Vein Endothelial Cells (HUVEC, PCS-100-010, ATCC, Manassas, VA, USA) were cultured on 1% Gelatin (G9136, Sigma-Aldrich, St. Louis, MO, USA) coated T75 flasks in Endothelial Cell Growth Medium MV2 (C-22022, PromoCell, Heidelberg, Germany). HBMECs and HUVECs were used between passages 4 and 10. C57BL/6 Mouse Embryonic Brain Endothelial Cells (C57-6023E,

Cell Biologics, Chicago, IL, USA) and Aged Mouse Brain Microvascular Endothelial Cells (A57-6023, Cell Biologics, Chicago, IL, USA) were cultured on 1% Gelatin coated T75 flasks and grown in complete Endothelial Cell Medium (1001, ScienCell, Carlsbad, CA, USA). All cells were cultured at 37°C and 5% CO_2.

Cell Transductions and Transfections

Stable transduction of miRs: VSV-G-pseudotyped lentiviral particles were made by transfecting 5.3 µg of pMD2-G (12259, Addgene, Watertown, MA, USA), 9.7 µg of pCMV-DR8.74 (8455, Addgene, Watertown, MA, USA), and 15 µg of pCD510B-1 (miR Control), mZIP, pCD510B-1-miR-23b, or mZIP-anti-miR-23b into 293T cells using Lipofectamine LTX (15338030, ThermoFisher, Waltham, MA, USA). Viral supernatants were concentrated using PEG-it (LV810A-1, System Biosciences, Palo Alto, CA, USA). Cells were transduced with high-titer virus using polybrene (sc134220, Santa Cruz Biotech, Dallas, TX, USA) and spinoculated at 800 × g at 32°C for 30 minutes. HBMEC and hCMEC/D3 transduced cells were selected at 48 hours and maintained with 1 or 3 µg/mL puromycin (J67236.8EQ, ThermoFisher, Waltham, MA, USA), respectively.

miR mimic transfection: HUVECs were seeded at 300K/well in a 6-well plate and grown until confluent. Transfections were prepared using Lipofectamine™ RNAiMAX Transfection Reagent kit (13778030, ThermoFisher, Waltham, MA, USA) and using both Anti-miR™ miRNA-23b Inhibitor (AM17000, ThermoFisher) and Anti-miR™ miRNA Inhibitor Negative Control #1 (AM17010, ThermoFisher). The final miRNA concentration added to each well was 25 pmol/well, and the final Lipofectamine™ RNAiMAX added to each well was 7.5 µL/well.

Cell proliferation analysis

Cells were plated at low density (6-well plates at 2 × 104 cells/well) in triplicate and counted.

anti-miR lentiviral library screen

The Electrical Cell-Substrate Impedance Sensing system (ECIS ZΘ; Applied BioPhysics) was used to monitor transendothelial electrical resistance (TEER) in real time in 96-well plate format (96W20idf PET plates, Applied BioPhysics). The plates were stabilized with 10 mM L-Cysteine (C6852, Sigma-Aldrich) coated with 100 µg/mL Poly-D-lysine (P6407, Sigma-Aldrich), then coated with 10 µg/mL fibronectin (F2006, Sigma-Aldrich). For all ECIS experiments, endothelial cells (ECs) were plated at 50,000 cells/well. TEER was measured at 4000 Hz for 72–96 hr. Mouse lung endothelial cells (mLECs) were plated at 10,000 cells per well in a 96-well plate, incubated with 8 µg/mL polybrene (SC-134220, Santa

Cruz Biotechnology) and transduced by spinoculation (800 x g at 32°C for 30 min) with the miRZipTM anti-miR lentiviral library (MZIPPLVA-1, System Biosciences) using 10,000 IFUs per well to ensure an MOI<1. Puromycin selection (1 µg/mL) was initiated 48 hours after transduction with full media changes every second day. Human lung endothelial cells (hLECs) were transduced with the miR overexpression and knockdown high-titer viruses and selected with 10 µg/ml puromycin, after which an ECIS experiment was performed.

TEER analysis – 2D and 3D

ECIS analysis. The Electrical Cell-Substrate Impedance Sensing system (ECIS ZΘ; Applied BioPhysics) was used to monitor transendothelial electrical resistance (TEER) in real time in 96-well plate format (96W20idf PET plates, Applied Biophysics). The plates were stabilized with 10 mM L-Cysteine (C6852, Sigma-Aldrich) coated with 100 µg/mL Poly-D-lysine (P6407, Sigma-Aldrich), then coated with 10 µg/mL fibronectin (F2006, Sigma-Aldrich). All ECIS experiments had lung endothelial cells (LECs) plated at 50,000 cells/well. TEER was measured at 4000 Hz for days to weeks.

EVOM3 analysis. Parental and miR-modulated HBMECs and HUVECs were both seeded on 15 µg/mL Fibronectin or 0.1% Gelatin-coated Transwell® inserts in a 12-well plate (3422, Costar) at 300K cells/well. Trans-endothelial electrical resistance (TEER) measurements were performed using an EVOM3 voltohmmeter (World Precision Instruments) at the start of culture and every 24 hours thereafter. Resistance values (Ω) were multiplied by 1.13cm^2, the surface area of the Transwell® insert, to obtain TEER values (Ω x cm^2). TEER values of an empty insert were subtracted from each measurement.

OrganoTEER- 3D TEER. HBSS was added to the middle and bottom channel inlets and outlets (50µL) of the OrganoPlate 3-lane 40/64-chip cultures, and fresh HBMEC-BM was added to the top channel inlets and outlets (50µL). The OrganoTEER device was placed on top of the OrganoPlate, and continuous TEER (Ω x cm^2) measurements were taken every 8 minutes using the "low TEER" setting. Alternatively, snapshot TEER measurements were performed intermittently, when multiple chip culture plates were analyzed in parallel.

Brain EC miR Profiling

Total RNA was isolated from HBMECs, Mouse Embryonic Brain ECs, and Aged Mouse Brain ECs following the manufacturer's protocol from *mir*Vana™ miRNA Isolation Kit (AM1560, ThermoFisher, Waltham, MA, USA). Total RNA was quantified using a NanoPhotometer (IMPLEN, Munich, Germany). Next, cDNA was made using miRCURY LNA RT Kit (339340, Qiagen, Venlo, Netherlands) and qPCR

was carried out using the miRCURY LNA SYBR Green PCR Kit (339346, Qiagen, Venlo, Netherlands) and the following miRCURY LNA miRNA PCR Assays from Qiagen: hsa-miR-181d-5p (YP00204789), hsa-miR-149-5p (YP00204321), hsa-miR-24-3p (YP00204260), has-miR-9-5p (YP00204513), has-miR-126-5p (YP00206010), has-miR-21-5p (YP00204230), has-miR-17-5p (YP02119304), hsa-let-7b-3p (YP00205653), hsa-miR-23a-3p (YP00204772), hsa-miR-27b-3p (YP00205915), hsa-miR-23b-3p (YP02119314), hsa-miR-29a-3p (YP00204698), hsa-miR-24-1-5p (YD00610842), hsa-miR-301a-3p (YP00205601) and RNU1A1 (YP00203909), on a StepOnePlus™ Real-Time PCR System (4376600, Applied Biosystems, Waltham, MA, USA). All miRCURY LNA miRNA PCR Assays were confirmed to target human and mouse sequences. Each assay was carried out in triplicate, and gene expression for each miR was normalized to the reference gene RNU1A1.

Western Blotting

Cells were lysed in cold RIPA buffer (89901, ThermoFisher, Waltham, MA, USA) containing protease inhibitor cocktail (PI78410, ThermoFisher) to extract protein. Samples containing 1x LDS sample buffer (NP0008, ThermoFisher) were boiled at 95 °C for 5 minutes. SDS-PAGE was performed by loading samples on NuPAGE Novex 4-12% Bis–Tris Protein Gels (NP0335, ThermoFisher). Methanol-activated PVDF membranes (1704156EDU, Bio-Rad, Hercules, CA, USA) were used to transfer gel samples using the Trans-Blot Turbo Transfer System (1704150, Bio-Rad, Hercules, CA, USA). PVDF membranes were blocked for one hour with 5% non-fat milk (NC9952266, Lab Scientific, Waltham, MA, USA) and incubated overnight at 4°C with the following primary antibodies: ZO-1 (61-7300, Invitrogen, Waltham, MA, USA), Claudin-5 (35-2500, Invitrogen), Occludin (33-1500, Invitrogen), GAPDH (MA5-15738, Invitrogen), VE-cadherin (2500, Cell Signaling Technology, Danvers, MA, USA), PLVAP (HPA002279, Sigma-Aldrich, St. Louis, MO, USA), LEF1 (2230, Cell Signaling Technology, Danvers, MA, USA), β-catenin (AF1329, R&D systems, Minneapolis, MN, USA), Cav-1 (3267, Cell Signaling Technology, Danvers, MA, USA). PVDF membranes were washed three times with TBS (1706435, Bio-Rad, Hercules, CA, USA) containing 0.1% Tween (AAJ20605AP, Fisher Scientific, Waltham, MA, USA), then incubated for an hour at room temperature with the following secondary antibodies: Peroxidase AffiniPure™ Donkey Anti-Rabbit IgG (H+L) (711-035-152, Jackson ImmunoResearch, West Grove, PA, USA), Peroxidase AffiniPure™ Donkey Anti-Mouse IgG (H+L) (715-035-150, Jackson ImmunoResearch, West Grove, PA, USA), Goat IgG HRP-conjugated Antibody (HAF109, R&D systems, Minneapolis, MN, USA). After three additional TBST washes, Pierce ECL Western Blotting Substrate (32106, ThermoFisher, Waltham, MA, USA) and ChemiDoc MP (Bio-Rad, Hercules, CA, USA) gel-documentation system were used for protein expression imaging.

OrganoPlate HBMEC culture

All experiments used the Mimetas OrganoPlate 3-lane platform (4004-400B, MIMETAS, Leiden, Netherlands). ECM gel was prepared on ice using 100mM HEPES (B35110, R&D Systems, Minneapolis, MN, USA), 37 g/L $NaHCO_3$ (S5761, Sigma-Aldrich, St. Louis, MO, USA), 5mg/mL Human Collagen Type IV (C5533-5MG, Sigma-Aldrich, St. Louis, MO, USA), and 5mg/mL Cultrex 3-D Culture Matrix Rat Collagen I (3447-020-01, Sigma-Aldrich, St. Louis, MO, USA) in a 1:1:1.6:6.4 ratio. Then, 2 µL of ECM gel was dispensed into the middle channel inlet and incubated for 15 min at 37°C. After plate incubation, 50 µL of PBS was added to the middle inlet to prevent the gel from drying. Next, 40µL of coating solution containing 50µg/mL collagen type IV and 30µg/mL fibronectin in PBS was used to coat the top channel of every chip, and the plate was left to incubate at 37°C for 1-3 hours. After the coating was aspirated, the top channels were washed with 50µL of PBS. PBS in the top channel inlet was replaced with 50µL of OrganoMedium HBMEC-BM (MI-OM-HBBM, Leiden, Netherlands). An HBMEC cell suspension of 1.5 x 10^6 cells/mL was prepared in OrganoMedium HBMEC-BM, and 2µL of cells were seeded in each top channel outlet. The OrganoPlate was incubated statically, on its side, for 3 hours to allow cells to adhere to ECM, after which 50µL of OrganoMedium HBMEC-BM was added to the top channel outlets and the OrganoPlate was then placed on OrganoFlow L perfusion rocker (MI-OFPR-L, MIMETAS, Leiden, Netherlands) at a 7°inclination, 8-min interval. Medium was changed every 2-3 days by replacing the top channel OrganoMedium HBMEC-BM in the top channel inlets and outlets with fresh OrganoMedium HBMEC-BM.

Modeling Stroke in vitro

Stroke was modeled using a three-fold approach (hypoglycemia, hypoxia, and flow stasis) for 6 hours. First, hypoglycemic conditions were achieved by replacing OrganoMedium HBMEC-BM culture media with deoxygenated Glucose Free Endothelial Cell Medium (1001-GF, ScienCell, Carlsbad, CA, USA). Hypoxic conditions were achieved by placing the OrganoPlate in CellXpert® C170i (Eppendorf, Hamburg, Germany) cell culture incubator set at 1% O_2. Flow stasis was achieved by removing the OrganoPlate from the OrganoFlow rocker and placing it flat in the incubator. HBMEC barrier integrity was monitored throughout the study by OrganoTEER.

Transcytosis Assay

Cells grown in 2D monolayers were seeded at 50K cells per well (96-well plate) and cultured until confluent. First, cells were incubated with 50ug/mL Labeled Bovine Serum Albumin CF®594 Dye

Conjugate (20290, Biotium) at 37°C for 1 hour. For 3D cultures, media containing 50ug/mL Labeled BSA CF®594 Dye Conjugate was added to the top channel inlets and outlets of the OrganoPlate and was allowed to rock for 1 hour. Following incubation, cells were washed of excess BSA-594 and were analyzed for CF®594 Mean Fluorescence Intensity (MFI) using Cytation C10 confocal imager or fixed with 4% PFA and co-stained with an immunofluorescence antibody.

Tracer Barrier Integrity Assay

At least 12 hours after seeding the 3D OrganoPlate, 0.5µg/mL FITC-Dextran 150kDa (46946, Sigma Aldrich) in HBSS was introduced into the top channel inlets and outlets (40µL and 30µL). Middle and bottom channel inlets and outlets were filled with 20 µL HBSS. The OrganoPlate was then placed flat for 15 minutes to allow tracer medium to perfuse through the top channel. Fluorescence intensity was measured via an EVOS microscope or Cytation C10 confocal plate reader. Analysis was performed by normalizing the average intensity of the middle and bottom channels over the intensity of the top channel, which represents leakage from the vascular (top) channel into the brain (middle and bottom) channels.

Immunocytochemistry

HBMECs in the OrganoPlate or on 96-well imaging plates (#655090, Greiner, Kremsmünster, Austria) were fixed with 4% paraformaldehyde in PBS or 100% methanol (-20°C), and permeabilized with 0.2% Triton X-100. Cells were incubated with blocking solution (2% FBS, 2% bovine serum albumin (0332-25G, VWR, Radnor, PA, USA), 0.1% Tween-20) for 30 minutes. Cells were incubated in the following primary antibodies diluted in blocking solution: ZO-1 Monoclonal Antibody (33-9100, Invitrogen, Waltham, MA, USA), Claudin-5 Monoclonal Antibody (35-2500, Invitrogen), VE-Cadherin Monoclonal Antibody (2500, Cell Signaling Technologies), PLVAP (HPA002279, Sigma-Aldrich, St. Louis, MO, USA), LEF1 (2230, Cell Signaling Technology), β-catenin (AF1329, R&D systems, Minneapolis, MN, USA) for 1-2 hours at room temperature, followed by incubation in the following Alexa Fluor-conjugated secondary antibodies: Goat anti-Mouse IgG (H+L) Cross-Adsorbed Secondary Antibody, Alexa Fluor™ 488 (A-11001, Invitrogen, Waltham, MA, USA), Goat anti-Mouse IgG (H+L) Cross-Adsorbed Secondary Antibody, Alexa Fluor™ 594 (A-11005, Invitrogen), Donkey anti-Goat IgG (H+L) Cross-Adsorbed Secondary Antibody, Alexa Fluor™ 647 (A-21447, Invitrogen), Donkey anti-Mouse IgG (H+L) Highly Cross-Adsorbed Secondary Antibody, Alexa Fluor™ 555 (A-31570, Invitrogen), Donkey anti-Goat IgG (H+L) Cross-Adsorbed Secondary Antibody, Alexa Fluor™ 594 (A-11058, Invitrogen), Donkey anti-Rabbit IgG (H+L) Highly Cross-Adsorbed Secondary Antibody, Alexa Fluor™ 488 (A-21206, Invitrogen)

for 30 minutes at room temperature. Nuclei were stained with DAPI (62248, Thermo Fisher). Cells were imaged with BioTek Cytation C10 Confocal Imaging Reader using 20x objective or Leica DMI8 SP8 Confocal Microscope (Leica, Wetzlar, Germany) using 40x or 63x oil-immersion objectives.

AAV-BR1 anti-miR-23b or control AAV-BR1 Administration

To target the cerebral endothelium, we generated AAV-BR1 anti-miR-23b and miR control virus (AAV2-BR1 plasmids from Dr. Körbelin's lab). Initial dosing and safety analysis showed that a single dose (i.v.), ($10x^{11}$ gp/mouse) of AAVBR1 virus encoding anti-miR-23b-GFP (or -mCherry, -Luciferase) was effective (>90% transduction rate) when introduced into mice by retro-orbital injections and analyzed after 3 weeks, demonstrating specific expression in brain endothelium, when stained using podocalyxin a HBMEC marker and AAVBR1-GFP. As reported, the AAVBR1 virus remained expressed for a long time (>600 days). Mice were active and maintained a healthy weight following viral administration. Analysis of the peripheral immune response by cytokine profiling of plasma (ProcartaPlex 36-plex arrays) showed no significant changes in expression of various cytokines (IL-1β, IL-6, IFN-γ, TNF-α, IL-8, IL-10, or IL-12) after 3 months, supporting the notion that the virus is well-tolerated.

Transient Middle Cerebral Artery Occlusion (tMCAo)

12 to 14-week-old male mice weighing 25-30g were used. Briefly, mice were anesthetized with 1-2% isoflurane in 100% oxygen. After the surgical exposure, the right external and common carotid arteries were permanently ligated. Then, a reusable monofilament (Doccol Inc., catalog no. 70SPRe2045) was introduced into the right common carotid artery and advanced 9–10 mm beyond the carotid bifurcation into the right internal carotid artery. The core body temperature was checked by rectal probe and maintained at 36.5 ± 0.5°C by a heating pad and lamp throughout the surgery. A laser Doppler flowmeter measured the cerebral blood flow, and at least an 80% reduction compared to presurgical baseline values was achieved after the insertion of the filament. The flowmeter probe was placed 2mm posterior and 5-6 mm lateral to the bregma on the skull. The reperfusion was achieved by withdrawing the filament 75 min after the insertion. Following closure of the surgical wound, mice were returned to their cages with free access to water and food. Tissue was obtained 96 hrs post-tMCAo for some animals.

Immunohistochemistry

Following tMCAo, mice received a tail vein injection of 1% Biocytin-TMR in PBS. Animals were euthanized with isoflurane and perfused first with PBS, then with 4% PFA in PBS. Brains were fixed in 4% PFA for 24 hours, after which tissue was cryoprotected in 30% sucrose for 24-48 hrs and embedded

in Tissue-Tek OCT. Next, mouse brains were embedded in OCT and frozen for 24 hours at -80 °C. Brains were sectioned in 12 µm-thick coronal slices spanning all bregma regions of interest using a Leica cryostat. Streptavidin-Alexa594 was used to amplify the Biocytin-594 signal, and Alexa Fluor 488-conjugated goat anti-mouse IgG was used to visualize serum IgG leakage in brain sections. Blood vessels were labeled by immunofluorescence with a mouse Podocalyxin antibody. Sections were imaged with an upright Zeiss Axioimager and Biocytin-TMR, and IgG leakage was quantified with Fiji software.

Statistics

Data was analyzed using GraphPad Prism (version). Student's t-tests were used to calculate two-tailed P-values, and data are displayed as mean ± s.e.m. of technical or independent biological replicates (n) as indicated. Usually *P < 0.05, **P < 0.01, ***P< 0.001, or ****P < 0.0001.

RESULTS

Identification of anti-miR-23b as an enhancer of endothelial BBB properties.

miRs are key regulators of brain homeostasis and are frequently dysregulated in neurological disorders, making them attractive therapeutic targets[41-45]. To identify physiologically relevant miRs that influence BEC function, we used a non-biased, lentiviral-based anti-miR screen to identify conserved miRs that regulate endothelial barrier function by measuring trans-endothelial electrical resistance (TEER) as a functional readout. This approach leverages anti-miRs that neutralize endogenously expressed miRs, minimizing artifacts associated with ectopic overexpression. We previously validated this strategy by identifying miR-128 as a key regulator of reverse transcriptase-associated pathways, including LINE-1, telomerase, and HIV-1[46-50]. Mouse lung ECs were transduced with a lentiviral anti-miR library that co-expressed copGFP and a puromycin resistance cassette to facilitate selection. Following transduction, single-cell clones were isolated, and TEER was measured using electric cell-substrate impedance sensing (ECIS) instrument (**Figure 1A**). Three clones showed significantly increased TEER compared to controls (**Figure 1B**), and three anti-miRs were independently isolated from at least two different clones. Among these, anti-miR-151a and anti-miR-375 were identified as enhancers of cell junctions. We and others have previously shown that miR-151a and miR-375 play a role in tumorigenesis, and miR-151a functions as an onco-miR to promote cell migration, invasion, partial epithelial-to-mesenchymal transition in non-small cell lung cancer, and tumor-associated angiogenesis[51,52]. Importantly, this screen also identified anti-miR-23b as a potent enhancer of endothelial barrier properties. To validate these findings, we generated lentiviral constructs encoding

miR-23b, anti-miR-23b, and a control miR, and transduced human lung ECs. After puromycin selection, TEER measurements showed that anti-miR-23b significantly increased TEER relative to control or miR-23b-overexpressing lung ECs, whereas miR-23b expression decreased TEER (**Figure 1C**). Therefore, miR-23b seems critical to regulate the endothelial paracellular barrier of lung ECs.

To assess miR-23b relevance for brain ECs, we examined expression of several miRs in mouse and human brain ECs by qRT-PCR. miR-23b was enriched in young, compared to aged, mouse brain ECs, as well as in primary human BMECs (HBMECs) (**Figure 1D**), consistent with previous studies demonstrating miR-23b enrichment in the vasculature and specifically ECs[53]. miR-23b is part of the miR-23-27-24 cluster, with two paralogous clusters (miR-23a and miR-23b) arising from ancient gene duplication events on human chromosomes 9q22 and 19p13. miR-23a and miR-23b share an identical seed sequence but differ by one nucleotide[54], and both are expressed in the brain endothelium alongside miR-27 and miR-24 (**Figure 1D**)[53]. Next, we examined the functional impact of anti-miR-23b on barrier integrity in human umbilical vein endothelial cells (HUVECs) and primary HBMECs. In both cell types, anti-miR-23b significantly enhanced TEER compared to control miR or unmodified cells (**Figures 1E, F**). These data suggest that miR-23b is critical in regulating endothelial paracellular barrier permeability in multiple cell lines, including HBMECs.

Neutralizing miR-23b enhances barrier properties of HBMECs through upregulation of cell junction proteins.

The selective BBB permeability depends on specialized adherens (AJ) and tight junctions (TJ) and their associated proteins, including VE-cadherin, Claudin-5, Occludin, and ZO-1[55,56] (**Figure 2B**). We investigated whether miR-23b and anti-miR-23b modulate the expression of these junctional proteins in BECs. We generated both primary HBMECs and a human cerebral microvascular endothelial cell line (hCMEC/D3), which stably overexpressed anti-miR-23b, miR-23b, or a control miR using lentiviral transduction [transduction efficiency routinely exceeded 90% (data not shown)]. In parallel, HUVECs were transiently transfected with miR-23b, anti-miR-23b, or control miR. Western blot (WB) analysis assessed ZO-1, Claudin-5, and Occludin protein levels. Anti-miR-23b significantly upregulated all three TJ proteins in HBMECs and HCMED/D3 lines, whereas miR-23b overexpression reduced their levels compared to controls (**Figure 2A**). Next, we performed immunofluorescence (IF) staining in HUVECs and primary HBMECs to assess the subcellular localization of these junctional proteins. HBMECs and HCMED/D3 lines expressing anti-miR-23b showed robust expression of Claudin-5, Occludin, and ZO-1 at cell junctions (**Figure 2C**), consistent with enhanced barrier integrity. Similarly, IF and WB analyses

demonstrated that anti-miR-23b significantly increased VE-Cadherin levels at cell junctions in HBMECs compared to controls (**Figure 2D**). These findings suggest that anti-miR-23b enhances endothelial paracellular barrier properties by upregulating tight and adherens junction proteins. While previous studies by us and others have shown that miR-23b and other miRs regulate junctional protein expression in different cell types, including lung epithelium and generic ECs[52,57-59], these data confirm that neutralization of miR-23b in BECs is critical under physiological conditions to promote barrier maturation.

anti-miR-23b enhances 3D tubule formation and BBB properties of HBMECs.

Traditional two-dimensional (2D) endothelial monolayer cultures offer limited physiological relevance for studying the BBB. Three-dimensional (3D) systems with flow more accurately reflect *in vivo* vascular architecture and function, affecting the expression of proteins critical for BBB function[60]. To better assess the impact of anti-miR-23b on BBB integrity under dynamic 3D conditions, we employed a 3D HBMEC culture model using the Mimetas 40/64-chip 3-lane OrganoPlate microfluidic system (**Figure 3A**). This platform integrates tissue-level complexity with precise environmental control, allowing for reproducible and quantitative assessments of BBB properties across multiple chips. Each chip uses only ~30,000 HBMECs, enabling cost-effective feasibility and scalability. The OrganoPlate system facilitates gravity-driven fluid flow via platform tilting, creating physiologic shear stress critical for HBMEC maturation and function. Cells are seeded into the top channel (coated with Collagen IV (Col IV)/Fibronectin (FN)), and vessel-like structures form against an extracellular matrix (ECM) gel (Col I/IV, 80:20) in the middle lane (**Figure 3A**). Functional, leak-tight BBB tubules are visualized with fluorescent tracers perfused into the upper channel, and tubule integrity is monitored by OrganoTEER (**Figure 3A**). Barrier integrity (BI) assays using dextran tracers of various molecular weights confirm the selectivity and maturity of HBMEC tubules, which remain stable for over three weeks (**Figure 3A**).

To determine how anti-miR-23b affects 3D vascular formation and barrier function of HBMECs, we compared anti-miR-23b-expressing HBMECs to control cells in the 3D assay. Both groups formed morphologically intact tubules; however, IF staining for ZO-1, CLAUDIN-5, and VE-CADHERIN and confocal imaging using a C10 confocal imaging plate reader demonstrated intact, lumenized 3D tubules in anti-miR-23b cultures with significantly elevated expression of ZO-1, CLAUDIN-5, and VE-CADHERIN compared to controls (**Figure 3G**). BI analysis demonstrated that anti-miR-23b significantly accelerated the formation of leak-tight HBMEC tubules, and tighter paracellular barrier function was observed as early as 18 hours post-seeding. In contrast, control tubules remained permeable (**Figure**

3C). This observation was also supported by 3D TEER measurements with the OrganoTEER, which showed significantly higher resistance in anti-miR-23b cultures than parental and control-miR HBMECs (**Figure 3D**). We tracked TEER during the first 24 hours of tubule development to assess their establishment. anti-miR-23b significantly accelerated the onset of functional tubules compared to controls (**Figure 3E**). Moreover, anti-miR-23b also strengthened tubule resistance over three weeks in culture (**Figure 3F**). These results validate our findings from 2D cultures (**Figure 2**) and demonstrate that anti-miR-23b improves HBMEC barrier function and vessel maturation in a physiologically relevant 3D context. Moreover, neutralization of miR-23b enhanced the speed, tightness, and durability of the BBB-like vessel formation in a 3D microfluidic model by promoting junctional protein expression.

Neutralizing miR-23b enhances transcellular barrier properties by downregulating PLVAP.

In addition to TJ integrity, low rates of transcellular transport are essential to maintain BBB function[17,55]. Dysregulation of transcellular transport has been recognized as an early contributor to barrier breakdown following pathological insults such as stroke[61,62]. To assess whether anti-miR-23b modulates transcytosis in BECs, we examined levels of several proteins that regulate transcellular transport in anti-miR-23b-expressing and control HBMECs and hCMEC/D3 cell lines (**Figure 4B**). WB analysis revealed that anti-miR-23b significantly downregulated Plasmalemma Vesicle-Associated Protein (PLVAP), a marker of fenestrated ECs (**Figure 4A**). In contrast, Caveolin-1 (Cav-1) and Caveolin-2 (Cav-2, not shown) protein levels were not altered by anti-miR-23b expression (**Figure 4A**). We performed a transcellular uptake assay using fluorescently labelled albumin (albumin-Alexa594, red) to determine the functional consequences of PLVAP downregulation. After one hour of exposure, anti-miR-23b HBMECs showed a marked reduction in intracellular albumin-A594 signal compared to control cells, indicating reduced uptake (**Figure 4C**). Quantification confirmed a significant decrease in albumin uptake in anti-miR-23b cultures (**Figure 4D**). To independently validate this observation, we performed IF imaging of PLVAP and DAPI in anti-miR-23b versus control HBMEC cultures. Anti-miR-23b expression led to a modest but statistically significant reduction in PLVAP protein levels (**Figure 4D**), consistent with the WB findings. Therefore, in BECs, anti-miR-23b acts as a dual stablilizer of the BBB by downregulating PLVAP to reduce transcellular uptake and transport and by enhancing the expression and structural properties of junctional proteins.

Inhibiting miR-23b enhances barrier properties through Wnt/β-catenin-dependent and -independent mechanisms.

Wnt/β-catenin signalling plays a central role in promoting and maintaining BBB integrity[55,63,64]. Following CNS injury, Wnt/β-catenin signalling can be reactivated in response to injury, contributing to vascular repair[55]. Given its involvement in BBB preservation, pharmacological or genetic modulation of this pathway has shown promise in preclinical models of neurological disease, such as ischemic stroke[25-29]. To determine whether miR-23b regulates the Wnt/β-catenin pathway, we analyzed protein levels of β-catenin and its transcriptional coactivator LEF-1 in anti-miR-23b-expressing versus control ECs. WB analysis revealed that anti-miR-23b significantly increased both β-catenin and LEF-1 protein levels in hCMEC/D3, HUVEC, and HBMEC lines (**Figure 5A**). We next corroborated these findings using IF in 2D cultures and 3D HBMEC tubules. There was increased expression of β-catenin and LEF-1 in anti-miR-23b HBMECs compared to controls in both 2D and 3D models (**Figure 5B**). Together, these data demonstrate that miR-23b suppresses the Wnt/β-catenin pathway, and its neutralization via anti-miR-23b enhances Wnt/β-catenin activity by upregulating β-catenin and LEF-1 expression in BECs.

anti-miR-23b reduces BBB deficits in a 3D in vitro stroke-like model.

Ischemic stroke induces BBB dysfunction through a cascade of cellular events, including serum protein leakage, immune cell infiltration, and inflammation, that exacerbate neuronal damage[65-67]. Even subtle increases in BBB permeability can result in hippocampal injury and cognitive decline[68-72]. However, the underlying mechanisms of chronic BBB dysfunction in ischemic injury are not fully elucidated. We used our established 3D HBMEC culture platform to model ischemic stroke *in vitro* using the oxygen-glucose deprivation (OGD) paradigm. Baseline cultures of both anti-miR-23b and control HBMECs were established as leak-tight 3D tubules before OGD exposure (day 7–10). 3D HBMEC tubules were then exposed to hypoxia (1% O_2), glucose deprivation, and static flow for 6 hours, then returned to normoxic, glucose-replete conditions with restored flow (**Figure 6A**). This setup enabled us to assess both "acute injury" and "longer-term recovery" mechanisms related to BBB integrity. TEER analysis showed that while both groups exhibited a decline in barrier function during OGD, the loss was significantly less severe in anti-miR-23b cultures. Furthermore, anti-miR-23b cultures showed enhanced recovery following stroke-like injury (**Figure 6A**), suggesting a protective role for anti-miR-23b in injury resistance and barrier repair. BI assays further confirmed reduced BBB leakiness in anti-miR-23b cultures at both early (5 and 8 hours) and later timepoints (3 and 14 days) post-stroke-like conditions (**Figure 6B**).

Next, we examined TJ morphology of HBMEC 3D tubules during stroke-like conditions. While total expression and localization of Claudin-5, Occludin, and ZO-1 were not significantly altered during OGD,

structural analysis revealed a reduction in abnormal ZO-1$^+$ TJs with "zigzags" and gaps (green) in anti-miR-23b cultures, compared to controls, 21 days post-stroke (**Figure 6C**). These data suggest that anti-miR-23b preserves TJ morphological architecture even under hypoxic challenge. Because stroke is known to increase transcytosis[61], we measured albumin uptake with albumin-A594. anti-miR-23b HBMECs showed significantly reduced albumin uptake 5 hours post-OGD, relative to controls (**Figure 6D**). IF analysis also demonstrated decreased levels of PLVAP and intracellular albumin in anti-miR-23b cultures (**Figure 6D**), confirming suppression of transcytosis under ischemic conditions.

To investigate whether these are downstream of Wnt/β-catenin activity, we measured β-Catenin and LEF-1 proteins in anti-miR-23b and control cultures before and after OGD. LEF-1 expression was significantly reduced in both groups at 3 days post-stroke. However, by day 21, anti-miR-23b cultures exhibited robust expression of both β-catenin and LEF-1, in contrast to controls (**Figure 6E**). These findings suggest that anti-miR-23b not only preserves baseline Wnt/β-catenin signalling but also promotes its reactivation during later stages of BBB recovery. In summary, anti-miR-23b reduces BBB breakdown and accelerates barrier recovery in a 3D *in vitro* stroke-like model by preserving TJ structure, suppressing transcytosis, and enhancing Wnt/β-catenin signalling.

anti-miR-23b reduces stroke volume and neurological deficits in an in vivo ischemic stroke model.

Ischemic stroke causes irreversible damage to the infarct core and compromises the surrounding penumbra, a region considered therapeutically salvageable. BBB disruption is an early pathological feature that contributes to the conversion of the penumbra into the infarct core and is associated with a poor clinical outcome[73-75]. Because stroke-induced BBB disruption contributes directly to infarct expansion and cognitive decline, we asked whether anti-miR-23b could confer protection in a clinically relevant *in vivo* model of ischemic stroke. To assess the *in vivo* relevance of our *in vitro* findings, we conducted proof-of-concept studies using the transient middle cerebral artery occlusion (t-MCAO) stroke model, testing whether prophylactic treatment with anti-miR-23b could reduce BBB dysfunction and stroke severity. This stroke model induces transient cerebral ischemia in the cortex and striatum via insertion of an intraluminal suture into the internal carotid artery[61].

To selectively target brain ECs, we used an adeno-associated viral vector (AAV-BR1) developed by the Körbelin lab[76], which we engineered to express anti-miR-23b or a control miR. A single intravenous injection (10^{11} gp/mouse) via retro-orbital delivery resulted in >90% transduction efficiency in the brain endothelium, confirmed by co-staining with GFP (from AAV-BR1) and Podocalyxin, a

vascular marker (**Figure 7A**). The virus was well tolerated: mice maintained healthy body weight and cytokine profiling of the sera (IL-1β, IL-6, IFN-γ, TNF-α, IL-8, IL-10, or IL-12) revealed no significant systemic immune activation up to three months post-injection (data not shown). Therefore, AAV-BR1 is a suitable delivery platform for brain endothelial-specific gene expression of anti-miR-23b. To evaluate therapeutic potential, randomized adult male mice (3–4-month-old) were injected with AAVBR1-anti-miR-23b or control virus one week before the t-MCAO surgery (75 minutes of occlusion). Physiological parameters, including cerebral blood flow, temperature, and heart rate, were monitored blindly, and the immune status was assessed from plasma samples.

A subset of mice was sacrificed 96 hours post-t-MCAO to assess acute outcomes. The volume of BBB leakage was evaluated via serum IgG extravasation and biocytin-TMR (870 Da) tracer leakage administered intravenously 45 minutes before euthanasia (**Figure 7B**). There was extensive BBB leakage in the cortex of control mice. In contrast, prophylactic treatment with AAV-BR1-anti-miR-23b significantly reduced the area and the intensity of serum IgG and biocytin-TMR leakage (**Figure 7B & C**). Quantitative analysis revealed ~2-fold reductions in total BBB leakage volume and leakage area at several bregma regions (**Figure 7D & E**) and ~2-fold reductions in leakage intensity in anti-miR-23b-treated mice compared to controls (**Figure 7D & E**). In parallel, we assessed neurological scores and survival of mice. The percentage of animals exhibiting severe neurological impairment (score ≥5) was markedly lower in the anti-miR-23b group compared to controls (**Figure 7F**). Moreover, survival rates were improved in the anti-miR-23b-treated group, indicating at least some acute neuroprotection (**Figure 7G**).

In conclusion, prophylactic treatment with AAVBR1-delivered anti-miR-23b significantly reduced BBB leakage volume and leakage intensity as well as neurological deficits and mortality in the t-MCAO mouse stroke model, confirming the potential therapeutic effect of anti-miR-23b for ischemic stroke.

DISCUSSION

Acute BBB dysfunction, one of the earliest events in ischemic stroke, correlates strongly with poor outcomes[5-7]. Despite our understanding of the role of acute BBB dysfunction in ischemic stroke outcomes, the timing and mechanisms of BBB dysfunction and the optimal therapeutic strategies to prevent further damage and repair it remain poorly understood. In this study, we demonstrate that inhibition of miR-23b specifically in brain endothelium significantly enhances BBB resilience to damage and promotes its repair by activating both Wnt/β-catenin dependent and independent mechanisms.

Neutralizing miR-23b in BECs also increased the expression of critical BBB adherens (VE-Cadherin) and tight junction (ZO-1, Claudin-5, Occludin) proteins, and decreased transcellular transport through reduced expression of PLVAP. These effects were found in healthy conditions and under ischemic stress, improving BBB structural and functional integrity. Conversely, overexpression of miR-23b exacerbated BBB dysfunction, highlighting its role as a negative regulator of BBB integrity.

Utilizing an unbiased anti-miR screening strategy, we identified miR-23b as a conserved miR with potent regulator of endothelial barrier integrity. Other miRs, including miR-129, miR-221, and miR-191, have also been implicated in regulating vascular responses in stroke pathology, including angiogenesis, highlighting a complex miR regulatory network governing BBB function in neurological diseases[77-79]. However, these miRs were not identified in our anti-miR screening strategy for regulators specifically of endothelial barrier integrity. Our qRT-PCR analyses of several miRs revealed that miR-23a, miR-23b, and miR-27 (these miRs belong to the same cluster[54]) are highly expressed in young mouse BECs. Still, their levels are reduced in aged BECs, suggesting that downregulation in their expression may be a critical event in promoting the acquisition and maturation of barrier properties of brain endothelial cells. Our comprehensive mechanistic analyses confirm this hypothesis that miR-23b is an endogenously expressed miR that negatively regulates barrier integrity in multiple EC lines, including mouse and human BECs. miRs can function either by directly binding to and suppressing the translation of specific mRNAs or by targeting regulatory mRNAs that influence broader signalling pathways[80,81]. We performed bioinformatic analysis using TargetScanHuman and conducted preliminary miR-eCLIP (enhanced crosslinking and immune-purification) experiments to explore whether the observed effects stem from direct versus indirect regulation. Bioinformatic analyses and preliminary miR-eCLIP-seq data suggest that miR-23b directly targets VE-Cadherin, ZO-1, β-catenin, and LEF-1, whereas Claudin-5, Occludin, and PLVAP appear to be regulated indirectly through endothelial Wnt/β-catenin activity (data not shown). We cannot exclude the possibility that the expression of VE-Cadherin and ZO-1 may also be regulated indirectly by endothelial Wnt/β-catenin activity. Nevertheless, our data provide evidence that anti-miR-23b enhances BBB integrity through two mechanisms: first, directly relieving translational repression of two critical junctional and signalling proteins and second, promoting expression of additional BBB-associated genes indirectly through activation of endothelial Wnt/β-catenin signalling. Future eCLIP-seq experiments should help confirm these direct interactions and identify additional targets for miR-23b, providing further mechanistic understanding of miR-23b functions.

Several miRs have already been implicated in the regulation of stroke outcomes. miR-15a and miR-124 have been associated with ischemic stroke progression and protection, respectively[77,82-84]. miR-129, miR-221 and miR-191 regulate vascular responses during stroke pathology[77-79]. Our data expand the findings from previous reports that global, non-specific lentiviral inhibition of miR-23b alleviates ischemic injury by enhancing neuronal survival through the Nrf2 and c-Myc signalling pathways[85,86]. Notably, elevated serum levels of miR-23b-3p have been observed in patients with ischemic stroke and transient ischemic attack[86], suggesting a potential role in hypoxia-induced BBB disruption. However, miR-23 has also been reported to promote myelination and neuroprotection[87], suggesting a complex, yet paradoxical, role for miR-23b in neurons and oligodendrocytes. Our findings from both the *in vitro* 3D model of HBMEC tubules under stroke-like conditions as well as the *in vivo* stroke model (t-MCAO) using a brain endothelial-specific approach add significant insight into the mechanisms by which miR-23b neutralization may confer neuroprotection in ischemic stroke. Neutralization of miR-23b has a protective effect in both the BBB resistance to injury, as well as BBB repair after injury by regulating the expression of key BBB regulatory proteins (tight junctions and transcytosis), as well as affecting endothelial Wnt/β-catenin activity to promote BBB repair. Although our study primarily focuses on the role of miR-23b in regulating BBB integrity, additional research is necessary to explore its broader impact on other BEC functions relevant to stroke pathology, such as angiogenesis, immune cell infiltration, and vascular basement composition. Interestingly, existing literature shows conflicting roles for miR-23 in angiogenesis, suggesting context- and tissue-specific functions that warrant further investigation[53,88,89]. miR-23 has complex functions across various CNS disorders. While inhibiting miR-23b appears beneficial in stroke conditions, its induction has demonstrated neuroprotection in models of AD and traumatic brain injury[42,45,90-92]. Such disparities likely arise from distinct miR-23b targets and cell-type-specific responses, emphasizing the need for nuanced approaches when considering miR-based therapeutics.

A major barrier to understanding BBB pathology in stroke is the lack of human-relevant, high-fidelity *in vitro* models. Current *in vivo* models, including the tMCAo model, are valuable but limited by species-specific differences and labor-intensive methods that prevent extensive drug screening[93,94]. Our 3D microfluidic system, bridging more simplistic 2D assays and complex *in vivo* models, presents an ideal intermediate platform for studying stroke pathology and screening therapeutic candidates. Our 3D microfluidic BBB model significantly improves upon traditional 2D static cultures, offering a robust system for studying ischemic stroke mechanisms. Our studies demonstrate the value of this 3D BBB culture model as a predictive and mechanistically robust platform, enabling detailed exploration of brain

endothelial responses to ischemic injury and facilitating high-throughput screening of next-generation therapeutics. Our *in vivo* studies validate the protective effects observed in the *in vitro* 3D BBB model, demonstrating that endothelial-specific anti-miR-23b significantly reduces vascular leakage, preserves brain endothelial cell function, improves neurological outcomes, and enhances survival following tMCAo. These findings underscore the translational potential of anti-miR-23b as a therapeutic avenue for ischemic stroke. However, future enhancements incorporating BBB-supporting cells, such as PCs and ACs, along with other NVU and CNS components, including neurons and glial cells, will further increase physiological relevance and translational potential.

The potential therapeutic utility of anti-miR strategies is exemplified by existing miRNA-targeted therapies such as anti-miR-122 (Miravirsen), which has proven safe and effective against Hepatitis C[95-98]. Advanced delivery strategies, such as circular anti-miRs or nanoparticle-based approaches, could enhance therapeutic specificity and efficiency for CNS targeting. There is significant interest in identifying Wnt/β-catenin agonists capable of restoring homeostatic signalling without overstimulation to promote BBB repair, particularly in stroke. Recently, Wnt7a has been engineered to interact with Grp124/Reck to selectively target brain endothelial cells to promote Wnt/β-catenin signalling and BBB repair in ischemic stroke[28]. Targeting endogenous brain endothelial cell molecules, such as miR-23b, may offer another safe and effective strategy to achieve this therapeutic goal. Our targeted anti-miR-23b delivery via AAVBR1 specifically improved BBB integrity and neurological outcomes in the t-MCAo model through, in part, activation of Wnt/β-catenin signalling, suggesting clinical potential. Future research will explore post-stroke therapeutic interventions using anti-miR-23b, including evaluations in middle-aged and aged mice of both sexes. These studies will comprehensively assess neuronal injury, inflammation, immune cell infiltration, and long-term behavioural and cognitive outcomes, thus significantly advancing translational potential. Ultimately, RNA-based neuroprotection, such as anti-miR-23b, may offer long-term therapeutic benefits beyond conventional pharmacological interventions, which are limited by short durations in circulation. Local delivery techniques, such as catheter-based administration during mechanical thrombectomy, could facilitate clinical application.

In conclusion, given the broad implications of BBB dysfunction during aging and in various neurological disorders, including TBI, MS, AD, and NeuroHIV, our findings represent significant progress toward developing novel therapeutic small RNA-based strategies aimed at restoring BBB integrity and function across multiple CNS pathologies.

ACKNOWLEDGEMENT

The work of I.M. Pedersen is supported by the National Institutes of Health and DoD (grants R01 NS107344, R61R33 HL159949, HL159949-S1 and TP425-24-1-1046).
This is manuscript #1083 from Scintillon Research Institute.

AUTHOR CONTRIBUTIONS

V. Martinez designed and performed experiments and analyzed data. J. Krog and I. Daugaard performed experiments, and S. Nakanishi analyzed data. J. Körbelin provided AAVBR1 plasmids for AAVBR1 virus generation, V. Martinez and S. Nakanishi contributed to writing the methods sections of the manuscript. I.M. Pedersen designed all experiments, analyzed data, and wrote the paper with input from D. Agalliu and B. Lawson.

DECLARATION OF INTERESTS

Disclosures: J. Körbelin is listed as inventor on a patent on AAV-BR1 held by Boehringer Ingelheim Pharma. The other authors have nothing to declare.

REFERENCES

1. Zhao N, Chung TD, Guo Z, Jamieson JJ, Liang L, Linville RM, Pessell AF, Wang L, Searson PC. The influence of physiological and pathological perturbations on blood-brain barrier function. *Front Neurosci*. 2023;17:1289894. doi: 10.3389/fnins.2023.1289894
2. Sweeney MD, Zhao Z, Montagne A, Nelson AR, Zlokovic BV. Blood-Brain Barrier: From Physiology to Disease and Back. *Physiol Rev*. 2019;99:21-78. doi: 10.1152/physrev.00050.2017
3. Collaborators GBDS. Global, regional, and national burden of stroke, 1990-2016: a systematic analysis for the Global Burden of Disease Study 2016. *Lancet Neurol*. 2019;18:439-458. doi: 10.1016/S1474-4422(19)30034-1
4. Hoffmann A, Zhu G, Wintermark M. Advanced neuroimaging in stroke patients: prediction of tissue fate and hemorrhagic transformation. *Expert Rev Cardiovasc Ther*. 2012;10:515-524. doi: 10.1586/erc.12.30
5. Keep RF, Xiang J, Ennis SR, Andjelkovic A, Hua Y, Xi G, Hoff JT. Blood-brain barrier function in intracerebral hemorrhage. *Acta Neurochir Suppl*. 2008;105:73-77. doi: 10.1007/978-3-211-09469-3_15
6. Khatri R, McKinney AM, Swenson B, Janardhan V. Blood-brain barrier, reperfusion injury, and hemorrhagic transformation in acute ischemic stroke. *Neurology*. 2012;79:S52-57. doi: 10.1212/WNL.0b013e3182697e70
7. Prakash R, Carmichael ST. Blood-brain barrier breakdown and neovascularization processes after stroke and traumatic brain injury. *Curr Opin Neurol*. 2015;28:556-564. doi: 10.1097/WCO.0000000000000248
8. Anstey KJ, Ee N, Eramudugolla R, Jagger C, Peters R. A Systematic Review of Meta-Analyses that Evaluate Risk Factors for Dementia to Evaluate the Quantity, Quality, and Global Representativeness of Evidence. *J Alzheimers Dis*. 2019;70:S165-S186. doi: 10.3233/JAD-190181
9. Banks WA, Reed MJ, Logsdon AF, Rhea EM, Erickson MA. Healthy aging and the blood-brain barrier. *Nat Aging*. 2021;1:243-254. doi: 10.1038/s43587-021-00043-5
10. Beard JR, Officer A, de Carvalho IA, Sadana R, Pot AM, Michel JP, Lloyd-Sherlock P, Epping-Jordan JE, Peeters G, Mahanani WR, et al. The World report on ageing and health: a policy framework for healthy ageing. *Lancet*. 2016;387:2145-2154. doi: 10.1016/S0140-6736(15)00516-4
11. Boehme AK, Esenwa C, Elkind MS. Stroke Risk Factors, Genetics, and Prevention. *Circ Res*. 2017;120:472-495. doi: 10.1161/CIRCRESAHA.116.308398
12. Collaborators GBDS. Global, regional, and national burden of stroke and its risk factors, 1990-2019: a systematic analysis for the Global Burden of Disease Study 2019. *Lancet Neurol*. 2021;20:795-820. doi: 10.1016/S1474-4422(21)00252-0
13. Kennedy BK, Berger SL, Brunet A, Campisi J, Cuervo AM, Epel ES, Franceschi C, Lithgow GJ, Morimoto RI, Pessin JE, et al. Geroscience: linking aging to chronic disease. *Cell*. 2014;159:709-713. doi: 10.1016/j.cell.2014.10.039
14. Lopez-Otin C, Blasco MA, Partridge L, Serrano M, Kroemer G. The hallmarks of aging. *Cell*. 2013;153:1194-1217. doi: 10.1016/j.cell.2013.05.039
15. Menassa M, Stronks K, Khatmi F, Roa Diaz ZM, Espinola OP, Gamba M, Itodo OA, Buttia C, Wehrli F, Minder B, et al. Concepts and definitions of healthy ageing: a systematic review and synthesis of theoretical models. *EClinicalMedicine*. 2023;56:101821. doi: 10.1016/j.eclinm.2022.101821
16. Omura JD, McGuire LC, Patel R, Baumgart M, Lamb R, Jeffers EM, Olivari BS, Croft JB, Thomas CW, Hacker K. Modifiable Risk Factors for Alzheimer Disease and Related Dementias Among

Adults Aged >/=45 Years - United States, 2019. *MMWR Morb Mortal Wkly Rep*. 2022;71:680-685. doi: 10.15585/mmwr.mm7120a2
17. Yang AC, Stevens MY, Chen MB, Lee DP, Stahli D, Gate D, Contrepois K, Chen W, Iram T, Zhang L, et al. Physiological blood-brain transport is impaired with age by a shift in transcytosis. *Nature*. 2020;583:425-430. doi: 10.1038/s41586-020-2453-z
18. Ferrucci L, Fabbri E. Inflammageing: chronic inflammation in ageing, cardiovascular disease, and frailty. *Nat Rev Cardiol*. 2018;15:505-522. doi: 10.1038/s41569-018-0064-2
19. Franceschi C, Garagnani P, Parini P, Giuliani C, Santoro A. Inflammaging: a new immune-metabolic viewpoint for age-related diseases. *Nat Rev Endocrinol*. 2018;14:576-590. doi: 10.1038/s41574-018-0059-4
20. Furman D, Campisi J, Verdin E, Carrera-Bastos P, Targ S, Franceschi C, Ferrucci L, Gilroy DW, Fasano A, Miller GW, et al. Chronic inflammation in the etiology of disease across the life span. *Nat Med*. 2019;25:1822-1832. doi: 10.1038/s41591-019-0675-0
21. Lehallier B, Gate D, Schaum N, Nanasi T, Lee SE, Yousef H, Moran Losada P, Berdnik D, Keller A, Verghese J, et al. Undulating changes in human plasma proteome profiles across the lifespan. *Nat Med*. 2019;25:1843-1850. doi: 10.1038/s41591-019-0673-2
22. Sun Y, Koyama Y, Shimada S. Inflammation From Peripheral Organs to the Brain: How Does Systemic Inflammation Cause Neuroinflammation? *Front Aging Neurosci*. 2022;14:903455. doi: 10.3389/fnagi.2022.903455
23. Anrather J, Iadecola C. Inflammation and Stroke: An Overview. *Neurotherapeutics*. 2016;13:661-670. doi: 10.1007/s13311-016-0483-x
24. Biswas S, Cottarelli A, Agalliu D. Neuronal and glial regulation of CNS angiogenesis and barriergenesis. *Development*. 2020;147. doi: 10.1242/dev.182279
25. Lengfeld JE, Lutz SE, Smith JR, Diaconu C, Scott C, Kofman SB, Choi C, Walsh CM, Raine CS, Agalliu I, et al. Endothelial Wnt/beta-catenin signaling reduces immune cell infiltration in multiple sclerosis. *Proc Natl Acad Sci U S A*. 2017;114:E1168-E1177. doi: 10.1073/pnas.1609905114
26. Song S, Huang H, Guan X, Fiesler V, Bhuiyan MIH, Liu R, Jalali S, Hasan MN, Tai AK, Chattopadhyay A, et al. Activation of endothelial Wnt/β-catenin signaling by protective astrocytes repairs BBB damage in ischemic stroke. *Prog Neurobiol*. 2021;199:101963. doi: 10.1016/j.pneurobio.2020.101963
27. Corada M, Orsenigo F, Bhat GP, Conze LL, Breviario F, Cunha SI, Claesson-Welsh L, Beznoussenko GV, Mironov AA, Bacigaluppi M, et al. Fine-Tuning of Sox17 and Canonical Wnt Coordinates the Permeability Properties of the Blood-Brain Barrier. *Circ Res*. 2019;124:511-525. doi: 10.1161/circresaha.118.313316
28. Martin M, Vermeiren S, Bostaille N, Eubelen M, Spitzer D, Vermeersch M, Profaci CP, Pozuelo E, Toussay X, Raman-Nair J, et al. Engineered Wnt ligands enable blood-brain barrier repair in neurological disorders. *Science*. 2022;375:eabm4459. doi: 10.1126/science.abm4459
29. Ding J, Lee S-J, Vlahos L, Yuki K, Rada CC, van Unen V, Vuppalapaty M, Chen H, Sura A, McCormick AK, et al. Therapeutic blood-brain barrier modulation and stroke treatment by a bioengineered FZD4-selective WNT surrogate in mice. *Nature Communications*. 2023;14:2947. doi: 10.1038/s41467-023-37689-1
30. Bovari-Biri J, Garai K, Banfai K, Csongei V, Pongracz JE. miRNAs as Predictors of Barrier Integrity. *Biosensors (Basel)*. 2023;13. doi: 10.3390/bios13040422
31. Lopez-Ramirez MA, Reijerkerk A, de Vries HE, Romero IA. Regulation of brain endothelial barrier function by microRNAs in health and neuroinflammation. *FASEB J*. 2016;30:2662-2672. doi: 10.1096/fj.201600435RR
32. Todoran R, Falcione SR, Clarke M, Joy T, Boghozian R, Jickling GC. microRNA as a therapeutic for ischemic stroke. *Neurochem Int*. 2023;163:105487. doi: 10.1016/j.neuint.2023.105487
33. Agarwal V, Bell GW, Nam JW, Bartel DP. Predicting effective microRNA target sites in mammalian mRNAs. *Elife*. 2015;4. doi: 10.7554/eLife.05005

34. Baek D, Villen J, Shin C, Camargo FD, Gygi SP, Bartel DP. The impact of microRNAs on protein output. *Nature*. 2008;455:64-71. doi: 10.1038/nature07242
35. Lewis BP, Burge CB, Bartel DP. Conserved seed pairing, often flanked by adenosines, indicates that thousands of human genes are microRNA targets. *Cell*. 2005;120:15-20. doi: 10.1016/j.cell.2004.12.035
36. Friedman RC, Farh KK, Burge CB, Bartel DP. Most mammalian mRNAs are conserved targets of microRNAs. *Genome Res*. 2009;19:92-105. doi: 10.1101/gr.082701.108
37. Pedersen IM, Cheng G, Wieland S, Volinia S, Croce CM, Chisari FV, David M. Interferon modulation of cellular microRNAs as an antiviral mechanism. *Nature*. 2007;449:919-922. doi: 10.1038/nature06205
38. Pedersen IM, Otero D, Kao E, Miletic AV, Hother C, Ralfkiaer E, Rickert RC, Gronbaek K, David M. Onco-miR-155 targets SHIP1 to promote TNFalpha-dependent growth of B cell lymphomas. *EMBO Mol Med*. 2009;1:288-295. doi: 10.1002/emmm.200900028
39. Riess M, Fuchs NV, Idica A, Hamdorf M, Flory E, Pedersen IM, Konig R. Interferons Induce Expression of SAMHD1 in Monocytes through Down-regulation of miR-181a and miR-30a. *J Biol Chem*. 2017;292:264-277. doi: 10.1074/jbc.M116.752584
40. Tili E, Michaille JJ, Cimino A, Costinean S, Dumitru CD, Adair B, Fabbri M, Alder H, Liu CG, Calin GA, et al. Modulation of miR-155 and miR-125b levels following lipopolysaccharide/TNF-alpha stimulation and their possible roles in regulating the response to endotoxin shock. *J Immunol*. 2007;179:5082-5089. doi: 10.4049/jimmunol.179.8.5082
41. Du C, Liu C, Kang J, Zhao G, Ye Z, Huang S, Li Z, Wu Z, Pei G. MicroRNA miR-326 regulates TH-17 differentiation and is associated with the pathogenesis of multiple sclerosis. *Nat Immunol*. 2009;10:1252-1259. doi: 10.1038/ni.1798
42. Gangaraju VK, Lin H. MicroRNAs: key regulators of stem cells. *Nat Rev Mol Cell Biol*. 2009;10:116-125. doi: 10.1038/nrm2621
43. Hébert SS, Horré K, Nicolaï L, Papadopoulou AS, Mandemakers W, Silahtaroglu AN, Kauppinen S, Delacourte A, De Strooper B. Loss of microRNA cluster miR-29a/b-1 in sporadic Alzheimer's disease correlates with increased BACE1/beta-secretase expression. *Proc Natl Acad Sci U S A*. 2008;105:6415-6420. doi: 10.1073/pnas.0710263105
44. Ivey KN, Srivastava D. MicroRNAs as regulators of differentiation and cell fate decisions. *Cell Stem Cell*. 2010;7:36-41. doi: 10.1016/j.stem.2010.06.012
45. Lu M, Zhang Q, Deng M, Miao J, Guo Y, Gao W, Cui Q. An analysis of human microRNA and disease associations. *PLoS One*. 2008;3:e3420. doi: 10.1371/journal.pone.0003420
46. Bochnakian A, Zhen A, Zisoulis DG, Idica A, KewalRamani VN, Neel N, Daugaard I, Hamdorf M, Kitchen S, Lee K, et al. Interferon-Inducible MicroRNA miR-128 Modulates HIV-1 Replication by Targeting TNPO3 mRNA. *J Virol*. 2019;93. doi: 10.1128/JVI.00364-19
47. Fung L, Guzman H, Sevrioukov E, Idica A, Park E, Bochnakian A, Daugaard I, Jury D, Mortazavi A, Zisoulis DG, et al. miR-128 Restriction of LINE-1 (L1) Retrotransposition Is Dependent on Targeting hnRNPA1 mRNA. *Int J Mol Sci*. 2019;20. doi: 10.3390/ijms20081955
48. Guzman H, Sanders K, Idica A, Bochnakian A, Jury D, Daugaard I, Zisoulis DG, Pedersen IM. miR-128 inhibits telomerase activity by targeting TERT mRNA. *Oncotarget*. 2018;9:13244-13253. doi: 10.18632/oncotarget.24284
49. Hamdorf M, Idica A, Zisoulis DG, Gamelin L, Martin C, Sanders KJ, Pedersen IM. miR-128 represses L1 retrotransposition by binding directly to L1 RNA. *Nat Struct Mol Biol*. 2015;22:824-831. doi: 10.1038/nsmb.3090
50. Idica A, Sevrioukov EA, Zisoulis DG, Hamdorf M, Daugaard I, Kadandale P, Pedersen IM. MicroRNA miR-128 represses LINE-1 (L1) retrotransposition by down-regulating the nuclear import factor TNPO1. *J Biol Chem*. 2017;292:20494-20508. doi: 10.1074/jbc.M117.807677

51. Daugaard I, Sanders KJ, Idica A, Vittayarukskul K, Hamdorf M, Krog JD, Chow R, Jury D, Hansen LL, Hager H, et al. miR-151a induces partial EMT by regulating E-cadherin in NSCLC cells. *Oncogenesis*. 2017;6:e366. doi: 10.1038/oncsis.2017.66
52. Jury D, Daugaard I, Sanders KJ, Hansen LL, Agalliu D, Pedersen IM. miR-151a enhances Slug dependent angiogenesis. *Oncotarget*. 2020;11:2160-2171. doi: 10.18632/oncotarget.27331
53. Fridman R, Lacal JC, Reich R, Bonfil DR, Ahn CH. Differential effects of phorbol ester on the in vitro invasiveness of malignant and non-malignant human fibroblast cells. *J Cell Physiol*. 1990;142:55-60. doi: 10.1002/jcp.1041420108
54. Li J, Zhao Y, Lu Y, Ritchie W, Grau G, Vadas MA, Gamble JR. The Poly-cistronic miR-23-27-24 Complexes Target Endothelial Cell Junctions: Differential Functional and Molecular Effects of miR-23a and miR-23b. *Mol Ther Nucleic Acids*. 2016;5:e354. doi: 10.1038/mtna.2016.62
55. Liebner S, Dijkhuizen RM, Reiss Y, Plate KH, Agalliu D, Constantin G. Functional morphology of the blood-brain barrier in health and disease. *Acta Neuropathol*. 2018;135:311-336. doi: 10.1007/s00401-018-1815-1
56. Nag S. Morphology and molecular properties of cellular components of normal cerebral vessels. *Methods Mol Med*. 2003;89:3-36. doi: 10.1385/1-59259-419-0:3
57. Harati R, Hammad S, Tlili A, Mahfood M, Mabondzo A, Hamoudi R. miR-27a-3p regulates expression of intercellular junctions at the brain endothelium and controls the endothelial barrier permeability. *PLoS One*. 2022;17:e0262152. doi: 10.1371/journal.pone.0262152
58. Hsu YL, Hung JY, Chang WA, Lin YS, Pan YC, Tsai PH, Wu CY, Kuo PL. Hypoxic lung cancer-secreted exosomal miR-23a increased angiogenesis and vascular permeability by targeting prolyl hydroxylase and tight junction protein ZO-1. *Oncogene*. 2017;36:4929-4942. doi: 10.1038/onc.2017.105
59. Li J, Zhao Y, Choi J, Ting KK, Coleman P, Chen J, Cogger VC, Wan L, Shi Z, Moller T, et al. Targeting miR-27a/VE-cadherin interactions rescues cerebral cavernous malformations in mice. *PLoS Biol*. 2020;18:e3000734. doi: 10.1371/journal.pbio.3000734
60. Linville RM, Sklar MB, Grifno GN, Nerenberg RF, Zhou J, Ye R, DeStefano JG, Guo Z, Jha R, Jamieson JJ, et al. Three-dimensional microenvironment regulates gene expression, function, and tight junction dynamics of iPSC-derived blood-brain barrier microvessels. *Fluids Barriers CNS*. 2022;19:87. doi: 10.1186/s12987-022-00377-1
61. Knowland D, Arac A, Sekiguchi KJ, Hsu M, Lutz SE, Perrino J, Steinberg GK, Barres BA, Nimmerjahn A, Agalliu D. Stepwise recruitment of transcellular and paracellular pathways underlies blood-brain barrier breakdown in stroke. *Neuron*. 2014;82:603-617. doi: 10.1016/j.neuron.2014.03.003
62. Sadeghian H, Lacoste B, Qin T, Toussay X, Rosa R, Oka F, Chung DY, Takizawa T, Gu C, Ayata C. Spreading depolarizations trigger caveolin-1-dependent endothelial transcytosis. *Ann Neurol*. 2018;84:409-423. doi: 10.1002/ana.25298
63. Daneman R, Agalliu D, Zhou L, Kuhnert F, Kuo CJ, Barres BA. Wnt/beta-catenin signaling is required for CNS, but not non-CNS, angiogenesis. *Proc Natl Acad Sci U S A*. 2009;106:641-646. doi: 10.1073/pnas.0805165106
64. Garcia-Gallardo A, Campbell M. Understanding the Blood-Brain Barrier: From Physiology to Pathology. *Adv Exp Med Biol*. 2025;1477:1-33. doi: 10.1007/978-3-031-89525-8_1
65. Marshall RS. Progress in Intravenous Thrombolytic Therapy for Acute Stroke. *JAMA Neurol*. 2015;72:928-934. doi: 10.1001/jamaneurol.2015.0835
66. Wardlaw JM, Doubal FN, Valdes-Hernandez M, Wang X, Chappell FM, Shuler K, Armitage PA, Carpenter TC, Dennis MS. Blood-brain barrier permeability and long-term clinical and imaging outcomes in cerebral small vessel disease. *Stroke*. 2013;44:525-527. doi: 10.1161/STROKEAHA.112.669994
67. Zhang CE, Wong SM, van de Haar HJ, Staals J, Jansen JF, Jeukens CR, Hofman PA, van Oostenbrugge RJ, Backes WH. Blood-brain barrier leakage is more widespread in patients with

cerebral small vessel disease. *Neurology*. 2017;88:426-432. doi: 10.1212/WNL.0000000000003556
68. Cullen KM, Kocsi Z, Stone J. Pericapillary haem-rich deposits: evidence for microhaemorrhages in aging human cerebral cortex. *J Cereb Blood Flow Metab*. 2005;25:1656-1667. doi: 10.1038/sj.jcbfm.9600155
69. Farrall AJ, Wardlaw JM. Blood-brain barrier: ageing and microvascular disease--systematic review and meta-analysis. *Neurobiol Aging*. 2009;30:337-352. doi: 10.1016/j.neurobiolaging.2007.07.015
70. Fiala M, Liu QN, Sayre J, Pop V, Brahmandam V, Graves MC, Vinters HV. Cyclooxygenase-2-positive macrophages infiltrate the Alzheimer's disease brain and damage the blood-brain barrier. *Eur J Clin Invest*. 2002;32:360-371. doi: 10.1046/j.1365-2362.2002.00994.x
71. Hanyu H, Tanaka Y, Shimizu S, Takasaki M, Abe K. Cerebral microbleeds in Alzheimer's disease. *J Neurol*. 2003;250:1496-1497. doi: 10.1007/s00415-003-0245-7
72. Zlokovic BV. Neurovascular pathways to neurodegeneration in Alzheimer's disease and other disorders. *Nat Rev Neurosci*. 2011;12:723-738. doi: 10.1038/nrn3114
73. Bernardo-Castro S, Albino I, Barrera-Sandoval AM, Tomatis F, Sousa JA, Martins E, Simoes S, Lino MM, Ferreira L, Sargento-Freitas J. Therapeutic Nanoparticles for the Different Phases of Ischemic Stroke. *Life (Basel)*. 2021;11. doi: 10.3390/life11060482
74. Mosconi MG, Paciaroni M. Treatments in Ischemic Stroke: Current and Future. *Eur Neurol*. 2022;85:349-366. doi: 10.1159/000525822
75. Tuohy MC, Hillman EMC, Marshall R, Agalliu D. The age-dependent immune response to ischemic stroke. *Curr Opin Neurobiol*. 2023;78:102670. doi: 10.1016/j.conb.2022.102670
76. Körbelin J, Dogbevia G, Michelfelder S, Ridder DA, Hunger A, Wenzel J, Seismann H, Lampe M, Bannach J, Pasparakis M, et al. A brain microvasculature endothelial cell-specific viral vector with the potential to treat neurovascular and neurological diseases. *EMBO Mol Med*. 2016;8:609-625. doi: 10.15252/emmm.201506078
77. Du K, Zhao C, Wang L, Wang Y, Zhang KZ, Shen XY, Sun HX, Gao W, Lu X. MiR-191 inhibit angiogenesis after acute ischemic stroke targeting VEZF1. *Aging (Albany NY)*. 2019;11:2762-2786. doi: 10.18632/aging.101948
78. Lei Y, Jin X, Sun M, Ji Z. miR-129-5p Ameliorates Ischemic Brain Injury by Binding to SIAH1 and Activating the mTOR Signaling Pathway. *J Mol Neurosci*. 2021;71:1761-1771. doi: 10.1007/s12031-021-01872-0
79. Peng H, Yang H, Xiang X, Li S. MuicroRNA-221 participates in cerebral ischemic stroke by modulating endothelial cell function by regulating the PTEN/PI3K/AKT pathway. *Exp Ther Med*. 2020;19:443-450. doi: 10.3892/etm.2019.8263
80. Bartel DP. MicroRNAs: target recognition and regulatory functions. *Cell*. 2009;136:215-233. doi: 10.1016/j.cell.2009.01.002
81. Rigoutsos I. New tricks for animal microRNAS: targeting of amino acid coding regions at conserved and nonconserved sites. *Cancer Res*. 2009;69:3245-3248. doi: 10.1158/0008-5472.Can-09-0352
82. Doeppner TR, Doehring M, Bretschneider E, Zechariah A, Kaltwasser B, Muller B, Koch JC, Bahr M, Hermann DM, Michel U. MicroRNA-124 protects against focal cerebral ischemia via mechanisms involving Usp14-dependent REST degradation. *Acta Neuropathol*. 2013;126:251-265. doi: 10.1007/s00401-013-1142-5
83. Hu JJ, Qin LJ, Liu ZY, Liu P, Wei HP, Wang HY, Zhao CC, Ge ZM. miR-15a regulates oxygen glucose deprivation/reperfusion (OGD/R)-induced neuronal injury by targeting BDNF. *Kaohsiung J Med Sci*. 2020;36:27-34. doi: 10.1002/kjm2.12136
84. Wu J, Fan CL, Ma LJ, Liu T, Wang C, Song JX, Lv QS, Pan H, Zhang CN, Wang JJ. Distinctive expression signatures of serum microRNAs in ischaemic stroke and transient ischaemic attack patients. *Thromb Haemost*. 2017;117:992-1001. doi: 10.1160/TH16-08-0606

85. Xin R, Qu D, Su S, Zhao B, Chen D. Downregulation of miR-23b by transcription factor c-Myc alleviates ischemic brain injury by upregulating Nrf2. *Int J Biol Sci*. 2021;17:3659-3671. doi: 10.7150/ijbs.61399
86. Zhao Z, Guan JZ, Wu M, Lai GH, Zhu ZL. Downregulation of microRNA-23b protects against ischemia-reperfusion injury via p53 signaling pathway by upregulating MDM4 in rats. *J Cell Biochem*. 2019;120:4599-4612. doi: 10.1002/jcb.27748
87. Lin ST, Huang Y, Zhang L, Heng MY, Ptacek LJ, Fu YH. MicroRNA-23a promotes myelination in the central nervous system. *Proc Natl Acad Sci U S A*. 2013;110:17468-17473. doi: 10.1073/pnas.1317182110
88. Oikawa S, Wada S, Lee M, Maeda S, Akimoto T. Role of endothelial microRNA-23 clusters in angiogenesis in vivo. *Am J Physiol Heart Circ Physiol*. 2018;315:H838-H846. doi: 10.1152/ajpheart.00742.2017
89. Zhou Q, Gallagher R, Ufret-Vincenty R, Li X, Olson EN, Wang S. Regulation of angiogenesis and choroidal neovascularization by members of microRNA-23~27~24 clusters. *Proc Natl Acad Sci U S A*. 2011;108:8287-8292. doi: 10.1073/pnas.1105254108
90. Crooke ST, Witztum JL, Bennett CF, Baker BF. RNA-Targeted Therapeutics. *Cell Metab*. 2018;27:714-739. doi: 10.1016/j.cmet.2018.03.004
91. Fineberg SK, Kosik KS, Davidson BL. MicroRNAs potentiate neural development. *Neuron*. 2009;64:303-309. doi: 10.1016/j.neuron.2009.10.020
92. Khezri MR, Yousefi K, Zolbanin NM, Ghasemnejad-Berenji M. MicroRNAs in the pathophysiology of Alzheimer's disease and Parkinson's disease: an overview. *Mol Neurobiol*. 2022;59:1589-1603. doi: 10.1007/s12035-022-02727-4
93. Kumabe H, Masuda T, Ito S, Furihata T, Toda A, Mogi M, Araki N, Ohtsuki S. Proteome profile differences among human, monkey, and mouse brain microvessels and cultured brain microvascular endothelial cells. *Fluids Barriers CNS*. 2025;22:53. doi: 10.1186/s12987-025-00650-z
94. Song HW, Foreman KL, Gastfriend BD, Kuo JS, Palecek SP, Shusta EV. Transcriptomic comparison of human and mouse brain microvessels. *Sci Rep*. 2020;10:12358. doi: 10.1038/s41598-020-69096-7
95. Gebert LF, Rebhan MA, Crivelli SE, Denzler R, Stoffel M, Hall J. Miravirsen (SPC3649) can inhibit the biogenesis of miR-122. *Nucleic Acids Res*. 2014;42:609-621. doi: 10.1093/nar/gkt852
96. Lanford RE, Hildebrandt-Eriksen ES, Petri A, Persson R, Lindow M, Munk ME, Kauppinen S, Orum H. Therapeutic silencing of microRNA-122 in primates with chronic hepatitis C virus infection. *Science*. 2010;327:198-201. doi: 10.1126/science.1178178
97. van der Ree MH, Stelma F, Willemse SB, Brown A, Swadling L, van der Valk M, Sinnige MJ, van Nuenen AC, de Vree JML, Klenerman P, et al. Immune responses in DAA treated chronic hepatitis C patients with and without prior RG-101 dosing. *Antiviral Res*. 2017;146:139-145. doi: 10.1016/j.antiviral.2017.08.016
98. van der Ree MH, van der Meer AJ, de Bruijne J, Maan R, van Vliet A, Welzel TM, Zeuzem S, Lawitz EJ, Rodriguez-Torres M, Kupcova V, et al. Long-term safety and efficacy of microRNA-targeted therapy in chronic hepatitis C patients. *Antiviral Res*. 2014;111:53-59. doi: 10.1016/j.antiviral.2014.08.015

FIGURES AND FIGURE LEGENDS

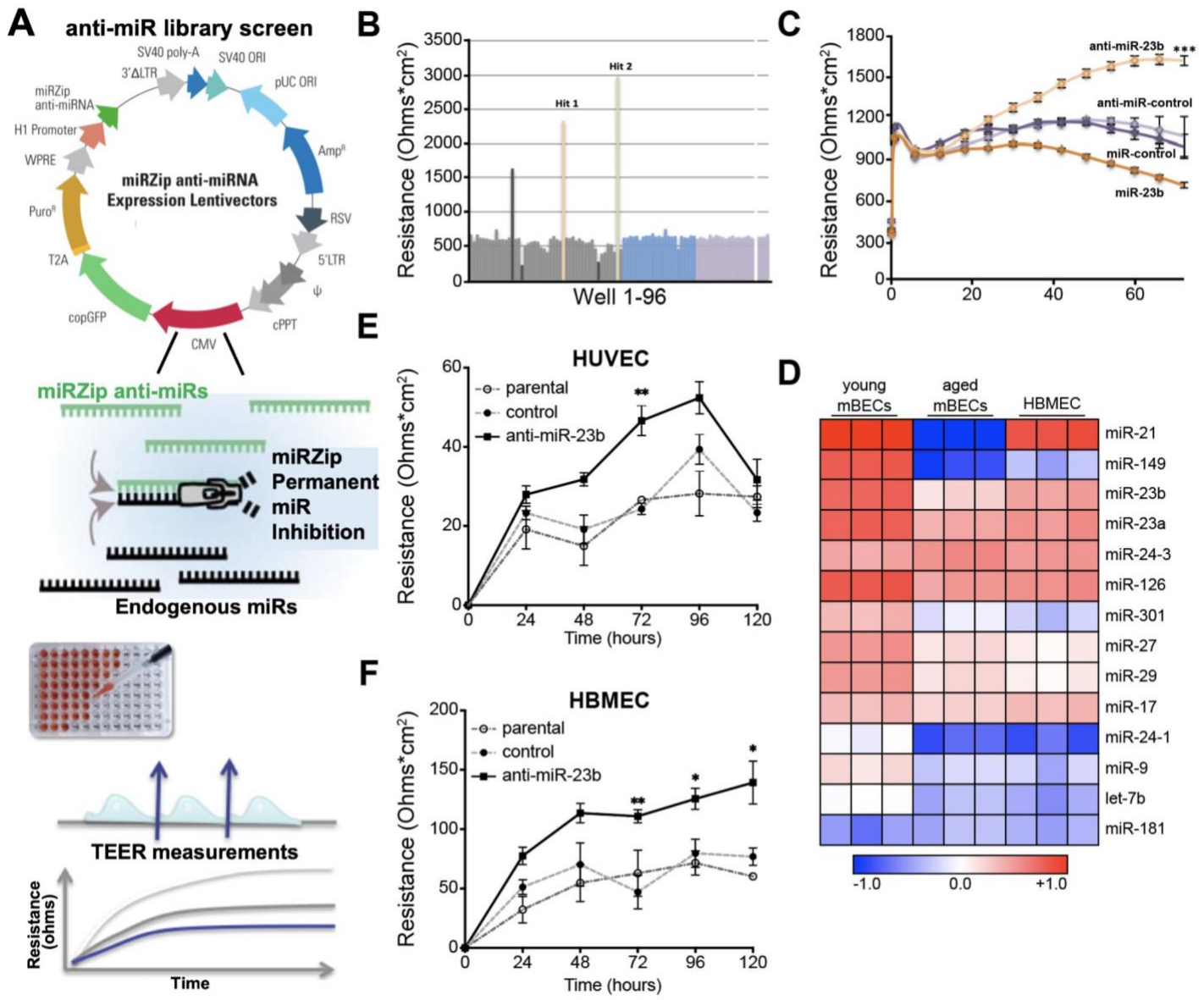

Figure 1. Identification of anti-miR-23b as a promoter of barrier properties in brain endothelial cells. (A) Schematic diagram of the anti-miR library screen to identify miRs/anti-miRs that regulate cell-cell contact and barrier properties in ECs. **(B)** Mouse lung endothelial cells were transduced using a lentiviral-based, miR-neutralizing shRNA library, selected for puromycin resistance, and clonally expanded. Each well represents the neutralization of a single endogenously expressed miR. Cells were then analyzed by trans-endothelial electrical resistance (TEER) by employing an Electric Cell-substrate Impedance Sensing (ECIS) plate reader to examine paracellular barrier properties. **(C)** Single high-titer miR-control, miR-23b, and anti-miR-23b lentiviruses were generated and stable miR-modulated human lung endothelial cells established. TEER was measured to assess the specific effect of miR-23b (n=12) **(D)** miR expression profiling was performed by miR specific qPCR analysis of mouse brain endothelial

cells (BECs) from postnatal pups and adult brains as well as primary human brain microvascular endothelial cells (HBMEC) and shown as a heatmap (n=3). **(E)** Human HUVECs were transfected with miR control or anti-miR-23b mimics (oligonucleotides), and **(F)** stable HBMECs (parental, miR control, and anti-miR-23b) were generated. HUVEC or HBMEC cells were subjected to TEER by ECIS or EVOM3 analysis (n=4). Results shown as percent change SEM ± n = 4 or 8, independent biological replicates, *$p < 0.05$, **$p < 0.01$, and ***$p < 0.001$ by two-tailed Student's t-test.

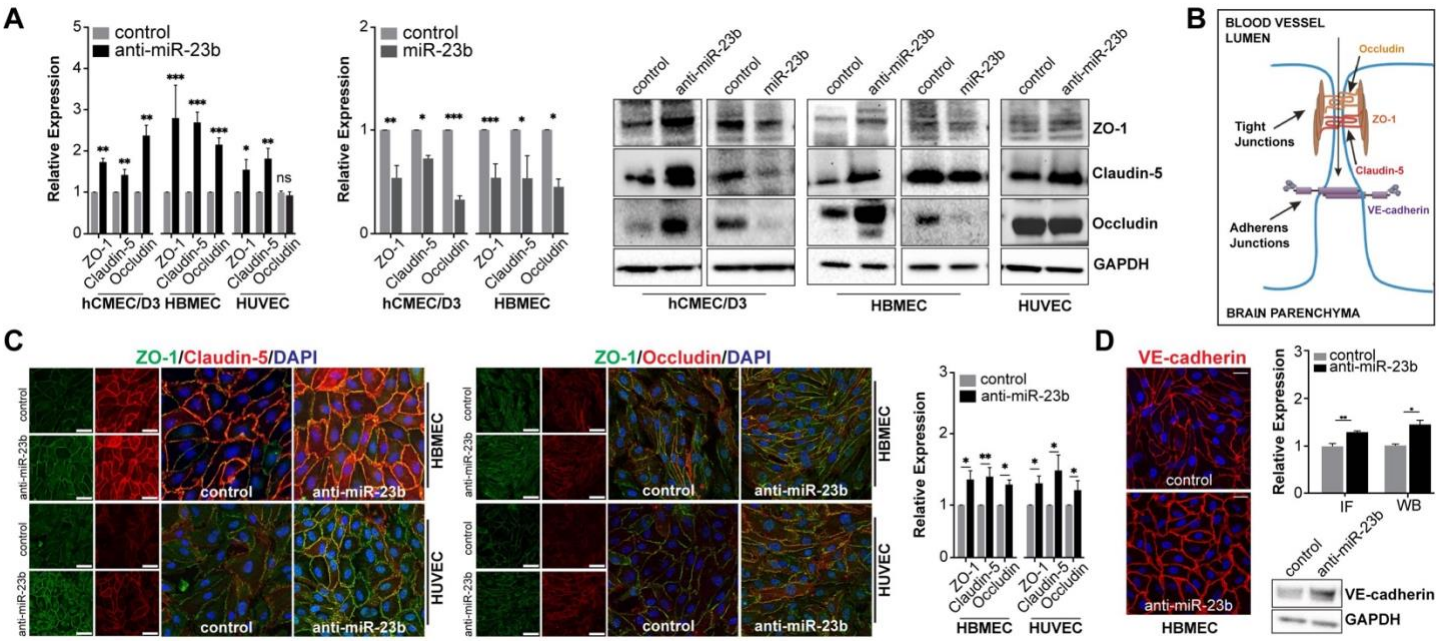

Figure 2. Anti-miR-23b enhances endothelial barrier properties through enhanced expression of cell junction proteins. (A) miR-modulated HBEMC or hCMEC/D3 lines were generated (over-expressing anti-miR-23b, miR-23b, or control miR), whereas HUVECs were transiently transfected with anti-miR-23b, miR-23b, or control miR oligonucleotides. Stable and transiently transduced anti-miR-23b, miR-23b, and control miR cell lines were analyzed for changes in protein levels of key tight junction proteins (ZO-1, Claudin-5, and Occludin) by Western blot (WB) analysis. Quantification of WB results (n = 3/sample) normalized to GAPDH is shown as relative levels (left), and representative examples are shown (right). **(B)** Cartoon of key brain endothelial cell junctional proteins. **(C)** Representative immunofluorescence (IF) images of transduced primary HBMECs and transiently transfected HUVECs stained for ZO-1 (green), Claudin-5 (red), and Occludin (red) are shown on the left, and the quantification of relative fluorescence levels is shown on the right. **(D)** Stable anti-miR-23b and control miR cell lines were analyzed for the adherens junction protein VE-Cadherin by IF (left panel), WB (right, bottom panel), and quantified (top, right panel). Graphs are shown as mean ± SEM (n = 3, independent biological replicates), *p <0.05, **p < 0.01, ***p < 0.001, by two-tailed Student's t-test.

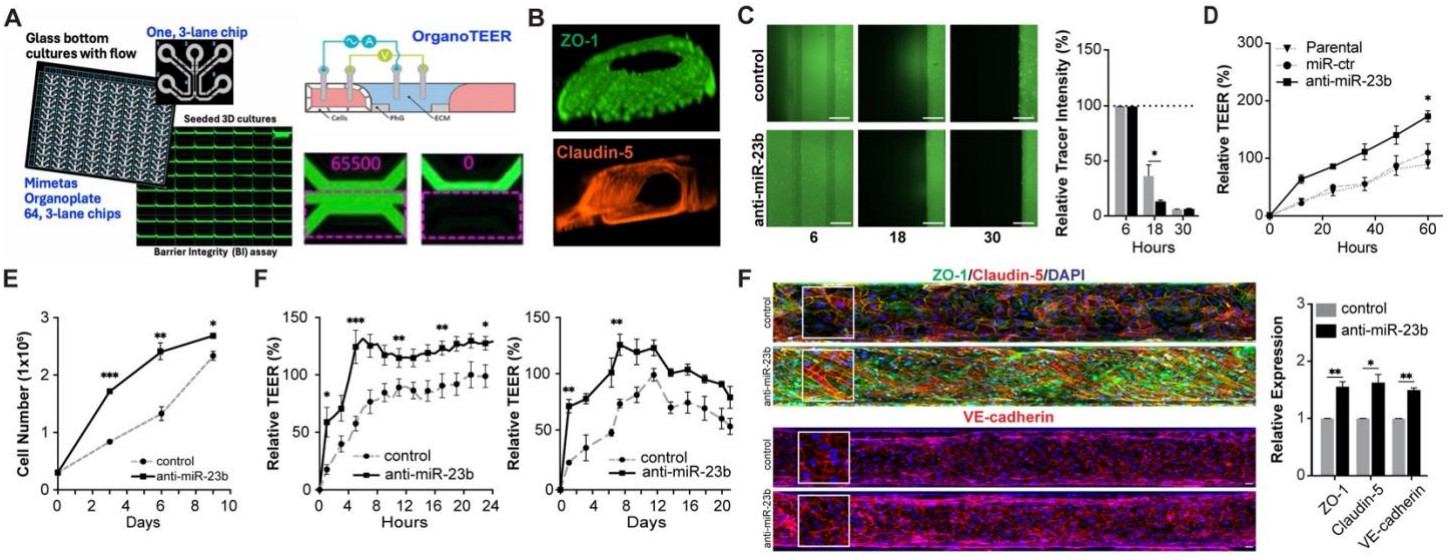

Figure 3. Anti-miR-23b enhances 3D tubule formation of HBMECs and their barrier properties. **(A)** Outline of the Mimetas organ-on-a-chip plate. Establishment of a perfused 3D tubule formed by primary HBMECs with flow using the Mimetas platform, which consists of 40 or 64 3-lane organ-on-a-chip, where each chip has three channels with a glass bottom. The top channel is seeded with HBMEC against the ECM (middle channel), allowing for 3D tubule formation of brain capillary size, and the bottom channel can be seeded with other CNS cells (pericytes or astrocytes). Intact HBMEC tubules in 64-chip visualized using 150KDa FITC-dextran tracer. Flow through the channels is introduced, and 3D TEER is measured continuously across the 3D tubule using the OrganoTEER instrument (top, right panel). Barrier integrity (BI) analysis is performed using different MW-sized tracers. A leaky 3D tubule will show tracer in the middle channel, whereas a functional, tight tubule only shows tracer in the top channel, mimicking a functional BBB (right, bottom panel). **(B)** Intact 3D HBMEC tubule formation is visualized by ZO-1 and Claudin-5 staining. **(C)** The timing of HBMECs tubule formation was examined using anti-miR-23b and miR control by BI analysis at 6, 18, and 30 hours (control is grey and anti-miR-23b is black). **(D)** 3D TEER analysis was performed on parental, control miR HBMECs, and anti-miR-23b HBMECs. **(E)** The proliferation potential of anti-miR-23b and control HBMECs was determined by cell counting of triplicate cultures, employing a cell coulter counter (n=5 replicates). **(F)** Plots of kinetic analysis of HBMEC tubule establishment (left panel) and long-term tubule resilience (right panel) were built from the TEER measurements (n=5 replicates). **(G)** IF staining for key junctional proteins [ZO-1 (green, top), Claudin-5 red, top), VE-Cadherin (red, bottom), and nuclear stain (DAPI)] in anti-miR-23b and control 3D HBMEC tubules. Representative images of the full top channel tubule and magnified images are shown in the left panels, and quantification is shown on the right (n=3 replicates). Graphs

are shown as mean ± SEM of 3 -5 independent biological replicates, *p <0.05, **p < 0.01, ***p < 0.001, ****p < 0.0001, by two-tailed Student's t-test.

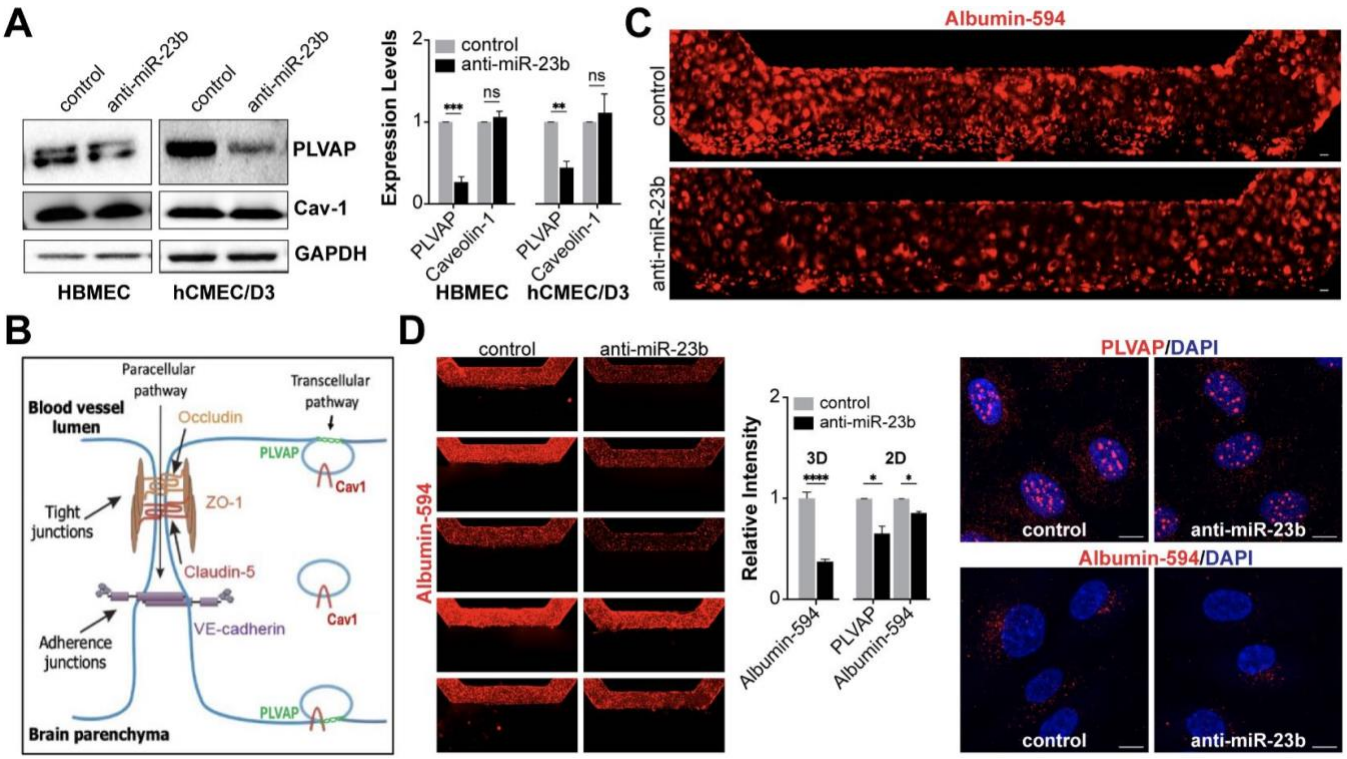

Figure 4. Anti-miR-23b enhances barrier properties by downregulating PLVAP and reducing transcytosis. (A) miR-modulated HBMEC or hCMEC/D3 lines were analyzed for changes in expression levels of Caveolin-1 and PLVAP by Western blotting. Representative examples are shown on the left, and quantification of results (n=3) normalized to GAPDH as relative levels are shown on the right. **(B)** Cartoon of brain endothelial cell junctional proteins and transcytosis, dependent on PVLAP expression. **(C, D)** Transcytosis assay employing labelled Albumin-594 (red), which is transported by transcytosis in HBMECs toward the brain using HBMECs overexpressing anti-miR-23b or controls. (**C**) Representative images of a single 3D tubule (top panel) and **(D, left)** complete 3-channel chip cultures (n=5), and quantification of albumin transcytosis (middle panel). (D, right) Confocal images of PLVAP/DAPI staining of anti-miR-23b or controls (right panel) and quantifications (middle panel). Graphs are shown as SEM ± of independent biological replicates, *p <0.05, **p < 0.01, ***p < 0.001, ****p < 0.0001, by two-tailed Student's t-test.

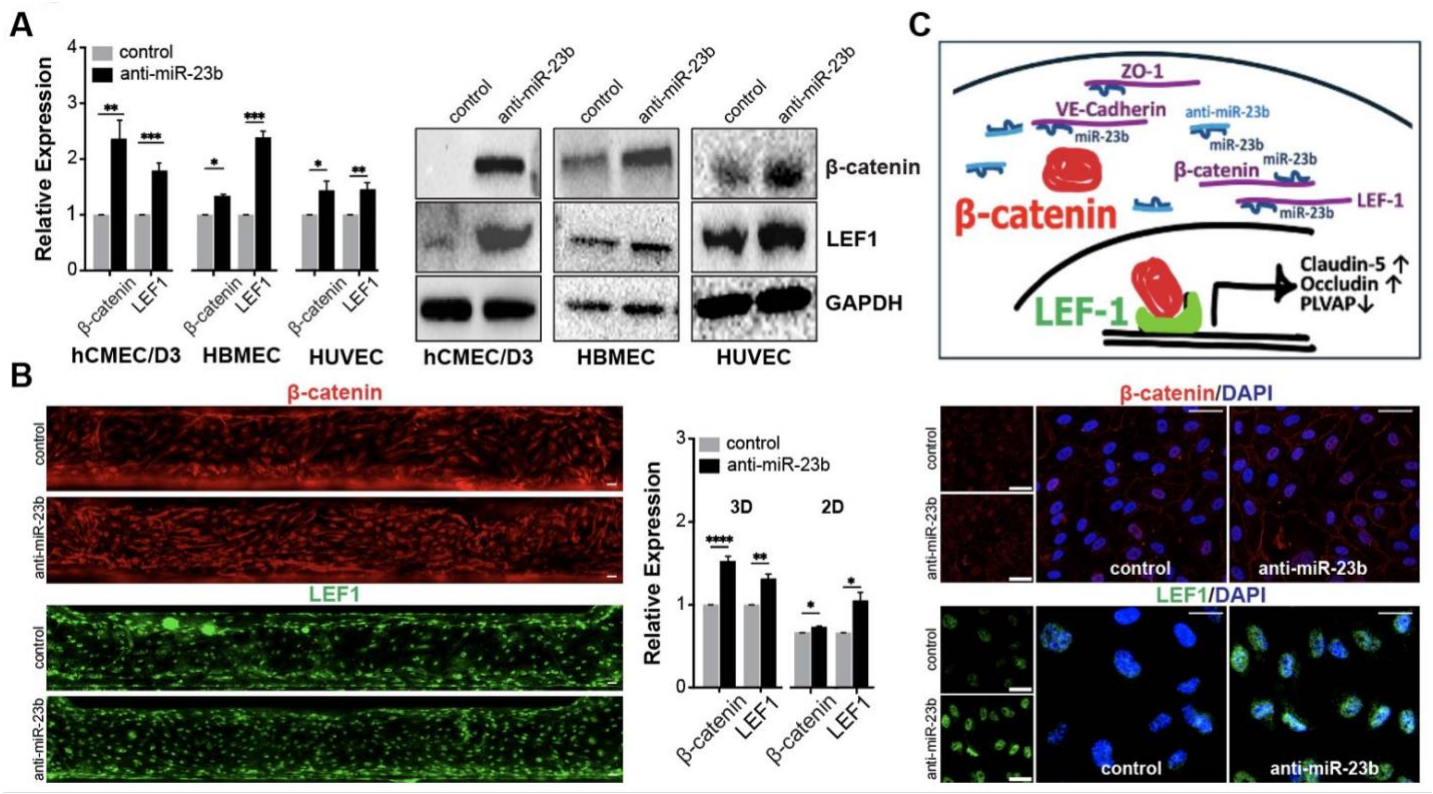

Figure 5. Anti-miR-23b enhances endothelial barrier properties through Wnt/β-catenin dependent and independent mechanisms. (A) Levels for β-catenin and LEF-1 proteins were determined by Western blot analysis in anti-miR-23b or control HBMEC, hCMEC/D3 lines, and transfected HUVECs. Results are quantified on the left, and representative images on the right, n=3 replicates. **(B)** Representative IF images of stable transduced HBMEC (anti-miR-23b and controls) stained for β-CATENIN (red) or LEF-1 (green) in 3D tubules (left panel), quantifications (middle panels), and magnification in 2D (right panel) and quantifications (middle panel). **(C)** Cartoon representation of miR/anti-miR-23b pathways, which are likely Wnt/β-catenin dependent. Graphs are shown as mean ± SEM of 3 independent biological replicates, *p <0.05, **p < 0.01, and ****p < 0.0001, by two-tailed Student's t-test.

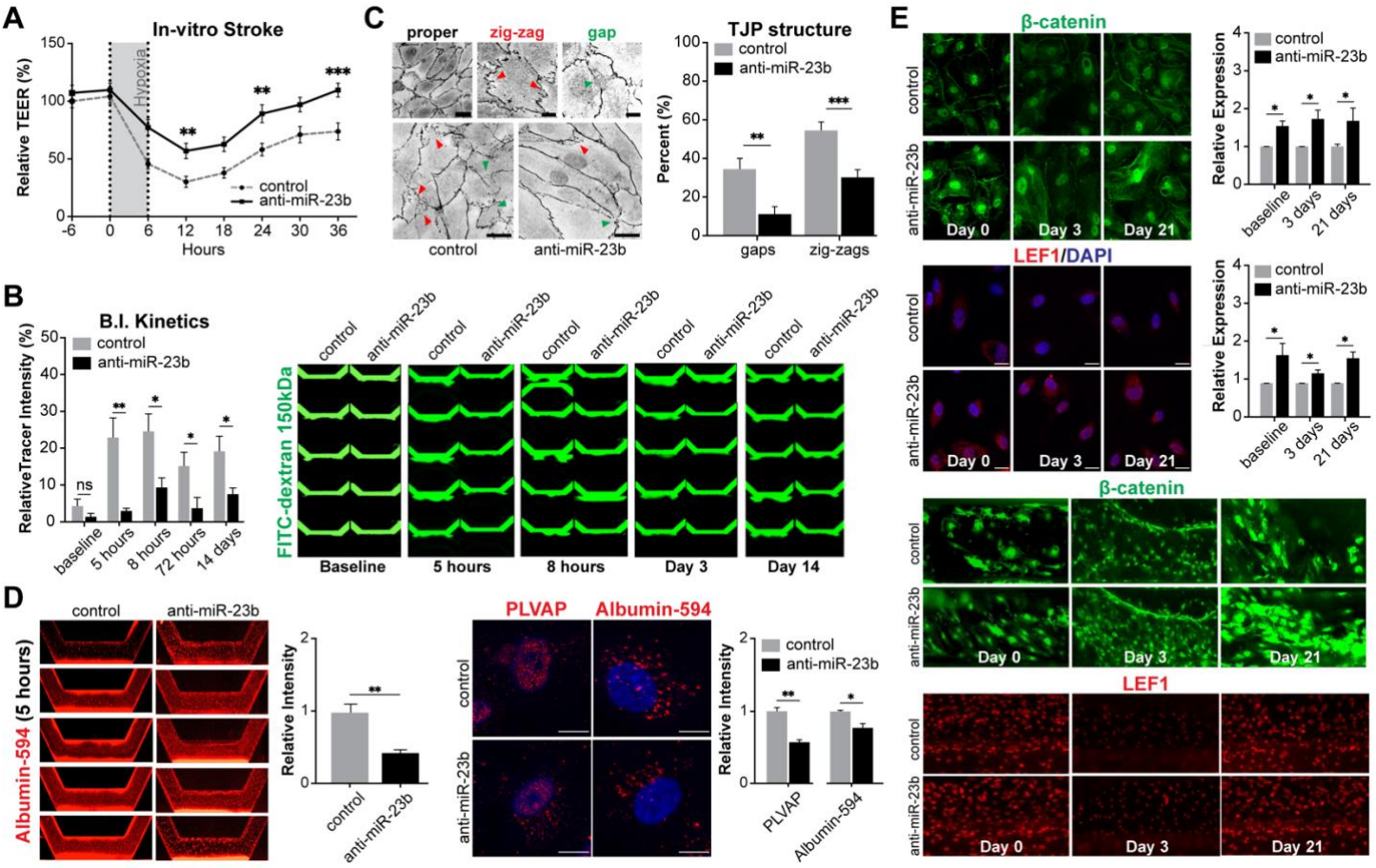

Figure 6. Anti-miR-23b reduces BBB deficits in a 3D *in vitro* stroke model. (A) anti-miR-23b or control HBMECs were seeded in the 3D Mimetas device. When 3D tubules were intact, cultures were exposed to *in vitro* stroke-like conditions (1% hypoxia, no glucose media, no/low flow). Continuous 3D TEER analysis shows partial loss of barrier function over time (n=10 chip cultures/condition). After 6 hours of *in-vitro* stroke-like conditions, cultures were rescued (moved to normoxia) with glucose, and the flow was reinstated, allowing for examination of resilience to *in-vitro* stroke-like conditions and BBB repair. **(B)** Measurements of tubule permeability were made using BI assays before, during, and following *in vitro* strokes using the C10 confocal imager. Representative images are shown for baseline, 5hrs, 8hrs, 72hrs, and 2 weeks after *in-vitro* stroke-like conditions (right panels), and quantifications of relative permeability (left graph) (n=10 chip cultures/condition/timepoint). **(C)** Tight junction morphology was analyzed by ZO-1 staining using the C10 confocal imager. The top panels show examples of intact tight junctions, junctions with zigzags, and junctions with gaps. Representative TJ morphology of anti-miR-23b or controls (left panel) on day 21 following *in vitro* stroke-like conditions (left) and quantifications (right), n=3 chips per condition. **(D)** Measurement of transcytosis of anti-miR-23b versus control HBMECs at 5 hours post *in vitro* stroke-like conditions. Shown are images of albumin-594 (red) transcytosis in chip images (left) and quantifications (middle left), and the right panel shows confocal

images of individual HBMECs for PLVAP, albumin-594 (middle right), and quantification (far right), n=5 chips per condition. **(E)** Activation of Wnt/β-catenin post *in vitro* stroke-like conditions was examined at baseline, at sub-acute (3 days) and at chronic time point (21 days) following in-vitro stroke by confocal analysis of β-catenin and LEF-1/DAPI of 3D cultures, magnified images (top left panel), quantifications (top, right panel) and tubule images (bottom panel), employing the C10 confocal imaging plate reader, n=5 chips per condition. Graphs are shown as mean ± SEM of 5 independent biological replicates, *$p < 0.05$, **$p < 0.01$, and ***$p < 0.001$, by two-tailed Student's t-test.

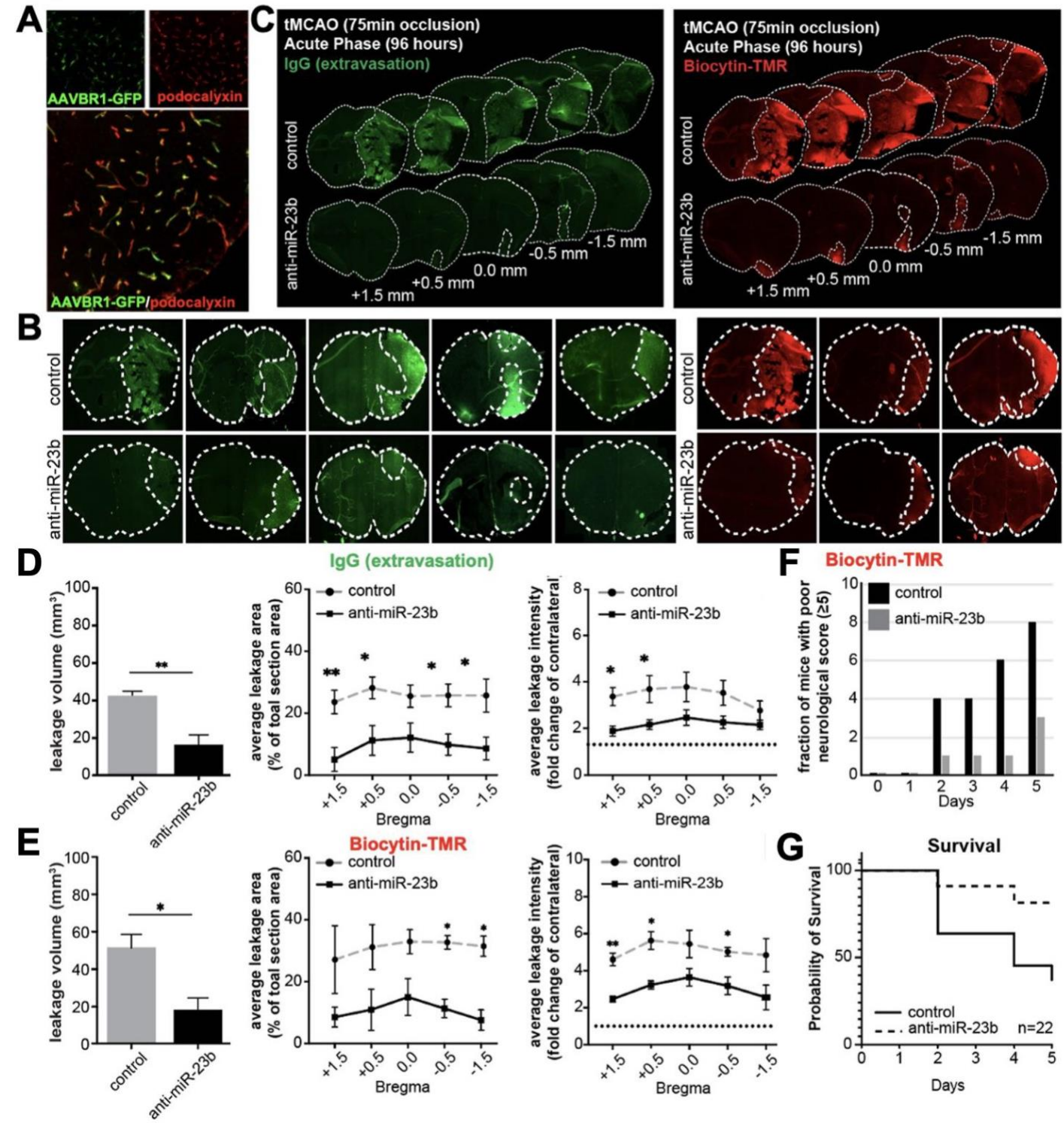

Figure 7. Endothelial anti-miR-23b overexpression before stroke reduces acute BBB leakage and neurological deficits following tMCAo. (A) Mice were transduced with AAVBR1 anti-miR-23b or control viruses before stroke to specifically and efficiently target endothelial cells long-term. A representative image of AAVBR1-control-GFP (green) virus showing expression in brain capillaries co-stained with podocalyxin (red, vessel marker), three weeks post-infection. **(B-C)** 20-week-old male mice

were injected with anti-miR-23b-AAVBR1 or control AAVBR1 7 days before the tMCAo surgery (75-minute occlusion). Some mice were sacrificed 4 days after tMCAo, and BBB damage was examined by analysis of serum IgG extravasation (green). **(D)** The leakage volume (left panel), average leakage area (middle panel), and average leakage intensity (right panel) for serum IgG extravasation (n=5 mice /group) are shown. **(E)** Some mice were exposed to tail-vein injections of a small tracer [biocytin-TMR (red); 890 Da] for 45 minutes before tissue harvest to visualize BBB permeability. Biocytin-TMR leakage volume (left panel), average leakage area (middle panel), and average leakage intensity (right panel) (n=3 mice/group). Finally, neurological scoring was monitored daily. A poor neurological score of> 5 is shown **(F),** and survival monitoring results are depicted in **(G)** (n=11 mice/group).